



Negative Modulation of Macroautophagy by Stabilized HERPUD1 is Counteracted by an Increased ER-Lysosomal Network With Impact in Drug-Induced Stress Cell Survival

OPEN ACCESS

Edited by:

Emily Eden,
University College London,
United Kingdom

Reviewed by:

Caroline Mauvezin,
University of Barcelona, Spain
Jieqiong Tan,
Central South University, China

*Correspondence:

Viviana A. Cavieres
vcavieres@docente.uss.cl
Patricia V. Burgos
patricia.burgos@uss.cl

[†]Present address: Institute of Biochemistry II,
School of Medicine, Goethe University
Frankfurt, Frankfurt, Germany

[‡]These authors contributed equally to this work

Specialty section:

This article was submitted to Membrane Traffic, a section of the journal *Frontiers in Cell and Developmental Biology*

Received: 18 July 2021

Accepted: 27 January 2022

Published: 02 March 2022

Citation:

Vargas G, Cortés O, Arias-Muñoz E, Hernández S, Cerda-Troncoso C, Hernández L, González AE, Tatham MH, Bustamante HA, Retamal C, Cancino J, Varas-Godoy M, Hay RT, Rojas-Fernández A, Cavieres VA and Burgos PV (2022) Negative Modulation of Macroautophagy by Stabilized HERPUD1 is Counteracted by an Increased ER-Lysosomal Network With Impact in Drug-Induced Stress Cell Survival. *Front. Cell Dev. Biol.* 10:743287. doi: 10.3389/fcell.2022.743287

Gabriela Vargas^{1‡}, Omar Cortés^{1‡}, Eloisa Arias-Muñoz^{1,2}, Sergio Hernández¹, Cristobal Cerda-Troncoso¹, Laura Hernández¹, Alexis E. González^{3†}, Michael H. Tatham⁴, Hianara A. Bustamante⁵, Claudio Retamal¹, Jorge Cancino¹, Manuel Varas-Godoy¹, Ronald T. Hay⁴, Alejandro Rojas-Fernández^{4,6}, Viviana A. Cavieres^{1,2*} and Patricia V. Burgos^{1,2,7*}

¹Centro de Biología Celular y Biomedicina (CEBICEM), Facultad de Medicina y Ciencia, Universidad San Sebastián, Santiago, Chile, ²Centro de Envejecimiento y Regeneración (CARE-UC), Facultad de Ciencias Biológicas, Pontificia Universidad Católica, Santiago, Chile, ³Facultad de Medicina, Instituto de Fisiología, Universidad Austral de Chile, Valdivia, Chile, ⁴Center for Gene Regulation and Expression, College of Life Sciences, University of Dundee, Dundee, United Kingdom, ⁵Facultad de Medicina, Instituto de Microbiología Clínica, Universidad Austral de Chile, Valdivia, Chile, ⁶Instituto de Medicina & Centro Interdisciplinario de Estudios del Sistema Nervioso (CISNe), Universidad Austral de Chile, Valdivia, Chile, ⁷Centro Ciencia & Vida, Fundación Ciencia & Vida, Santiago, Chile

Macroautophagy and the ubiquitin proteasome system work as an interconnected network in the maintenance of cellular homeostasis. Indeed, efficient activation of macroautophagy upon nutritional deprivation is sustained by degradation of preexisting proteins by the proteasome. However, the specific substrates that are degraded by the proteasome in order to activate macroautophagy are currently unknown. By quantitative proteomic analysis we identified several proteins downregulated in response to starvation independently of ATG5 expression. Among them, the most significant was HERPUD1, an ER membrane protein with low expression and known to be degraded by the proteasome under normal conditions. Contrary, under ER stress, levels of HERPUD1 increased rapidly due to a blockage in its proteasomal degradation. Thus, we explored whether HERPUD1 stability could work as a negative regulator of autophagy. In this work, we expressed a version of HERPUD1 with its ubiquitin-like domain (UBL) deleted, which is known to be crucial for its proteasome degradation. In comparison to HERPUD1-WT, we found the UBL-deleted version caused a negative role on basal and induced macroautophagy. Unexpectedly, we found stabilized HERPUD1 promotes ER remodeling independent of unfolded protein response activation observing an increase in stacked-tubular structures resembling previously described tubular ER rearrangements. Importantly, a phosphomimetic S59D mutation within the UBL mimics the phenotype observed with the UBL-deleted version including an increase in HERPUD1 stability and ER remodeling together with a negative role on autophagy. Moreover, we found UBL-deleted version and

HERPUD1-S59D trigger an increase in cellular size, whereas HERPUD1-S59D also causes an increased in nuclear size. Interestingly, ER remodeling by the deletion of the UBL and the phosphomimetic S59D version led to an increase in the number and function of lysosomes. In addition, the UBL-deleted version and phosphomimetic S59D version established a tight ER-lysosomal network with the presence of extended patches of ER-lysosomal membrane-contact sites condition that reveals an increase of cell survival under stress conditions. Altogether, we propose stabilized HERPUD1 downregulates macroautophagy favoring instead a closed interplay between the ER and lysosomes with consequences in drug-cell stress survival.

Keywords: HERPUD1, ubiquitin-like (UBL) domain, organelle network, lysosomal function, proteostasis, MCSs, ERAD (ER associated protein degradation)

INTRODUCTION

Macroautophagy (from here referred to as autophagy) is a catabolic pathway that mediates the engulfment of aberrant or damaged cytoplasmic constituents into double-membrane autophagosomes that subsequently fuse with lysosomes to form a hybrid organelle called the autolysosome that mediates the degradation of the cargo by acid hydrolases (Mizushima et al., 2008; Khaminets et al., 2016). Autophagy is also implicated in the degradation of cellular constituents under basal conditions, playing an essential role in the maintenance of cellular homeostasis upon a variety of environmental conditions such as nutrient restriction or other stressors (Murrow and Debnath, 2013). Autophagy is highly inducible by environmental changes being a very dynamic process that resolves a variety of cellular demands (Murrow and Debnath, 2013). In fact, increased autophagy is protective in different cells and organisms, playing a crucial role in cell maintenance and survival under different insults (Moreau et al., 2010). On the other hand, defects in autophagy enhance cell vulnerability under harmful conditions such as those present in the tumor microenvironment (Camuzard et al., 2020).

Although initially autophagy was thought to work independently of the ubiquitin proteasome system (UPS), increasing evidence shows many layers of both negative and positive regulation (Bustamante et al., 2018), revealing an interconnected network with important roles in cellular homeostasis and maintenance (Korolchuk et al., 2010). Inhibitors of the proteasome 20S catalytic core with the use of β -subunits blockers triggers an enhancement in the biogenesis of autophagosomes (Zhu et al., 2010). In contrast, impairment of the proteasome 19S regulatory particle with an inhibitor of PSMD14, a proteasomal deubiquitinating enzyme, blocks the biogenesis of autophagosomes (Demishtein et al., 2017; Bustamante et al., 2020). To date a limited number of substrates of the UPS system are known to play a regulatory role in autophagy (Jia and Bonifacino, 2019; Thayer et al., 2020) and many aspects about the functional role of this interconnected network between autophagy and UPS remain elusive.

To identify UPS substrates that could act as negative regulators of autophagy, we conducted a quantitative SILAC proteomic analysis in cells stably depleted of ATG5 by shRNA-mediated

knockdown. ATG5 protein is part of a complex with ATG12 and ATG16L that controls an essential step in the autophagosome formation (Walczak and Martens, 2013). We focused on proteins downregulated in response to nutrient deprivation, but not because of autophagy activation. The protein with the most significant downregulation, in wild type and ATG5 depleted cells was the Homocysteine-responsive endoplasmic reticulum-resident ubiquitin-like domain (UBL) member 1 protein named as HERPUD1. This protein is a transmembrane ER-resident protein with low levels of expression due to its short half-life by rapid proteasomal degradation (Kokame et al., 2000; Sai et al., 2003).

Here, we found that stabilized HERPUD1 through the deletion of its UBL domain causes a decrease in basal and induced autophagy. Additionally, it promotes an ER remodeling independent of the unfolded protein response activation into stacked tubular structures resembling previously described tubular ER rearrangements. Furthermore, we uncovered that higher HERPUD1 stability has a positive impact in lysosomal function, promoting an expanded ER-lysosomal network. Further, combining bioinformatics and site-directed mutagenesis we found the phosphomimetic S59D mutant within the UBL domain of HERPUD1 mimics the effect of the UBL deletion. In fact, we observed the phosphomimetic S59D mutant reduces basal and induced autophagy and remodeling of the ER-lysosomal network with the presence of ER-lysosomal membrane-contact sites, together promoting drug-stress cell survival. These findings thus identify HERPUD1 as a hotspot platform to promote stress cell survival by inducing the remodeling of the ER-lysosomal network when autophagy slows down.

MATERIALS AND METHODS

Reagents

Bafilomycin A1 (BafA1, cat#B1793), tunicamycin (Tun, cat#T7765), thapsigargin (Tg, cat#T9033), cisplatin (CDDP, cat#479306), Sulforhodamine B (SRB, cat#230162), Earle's balanced salt solution (EBSS, Cat#E2888), puromycin dihydrochloride (cat#P8833), and protease inhibitors cocktail (cat#P8340) were purchased from Sigma-Aldrich (St. Louis,

MO, United States). MG132 (cat#474790) was purchased from Merck Millipore (Burlington, MA, United States). LysoTracker™ Red DND-99 (cat#L7528), 4',6-diamidino-2-phenylindole (DAPI) (cat#D-1306) and TRIzol™ (cat#15596018) were purchased from ThermoFisher Scientific (Waltham, MA, United States), Magic Red® (cat#6133) was purchased from Immunochemistry Technologies, LLC (Bloomington, IN, United States). The QuikChange II XL direct-mutagenesis kit was obtained from Stratagene (cat#200522, La Jolla, CA, United States) and the Vybrant Apoptosis Pacific Blue-annexin V kit and 7AAD from Invitrogen (cat#A35122). The siRNA against human HERPUD1 (cat#SASI_Hs01_00185592) was purchased from Sigma Aldrich. The siRNA control corresponded to a custom non-target sequence UUCUCCGAACGUGUCACGUU purchased from Dharmacon.

Antibodies

The following monoclonal antibodies were used: mouse anti- β -ACTIN clone BA3R (cat# MA5-15739, Thermo Fisher Scientific), mouse anti-XBP-1S clone E7M5C (cat#47134S, Cell Signaling Technology, Danvers, MA, United States), mouse anti-FLAG clone M2 (cat#F1804, Sigma Aldrich), mouse anti-VAP-A clone 4C12 (cat#sc-293278, Santa Cruz Biotechnology, INC), mouse anti-GRP78/BiP clone 40/BiP (cat# 610978, BD Biosciences, San Jose, CA, United States), mouse anti-LAMP1 clone H4A3 (cat# 610978, Developmental Studies Hybridoma Bank, Iowa City, IA, United States), rabbit monoclonal anti-CALNEXIN clone C5C9 (cat#2679S, Cell Signaling Technologies), rabbit monoclonal anti-ATF4 clone D4B8 (cat#11815S, Cell Signaling Technologies), rabbit monoclonal anti-HERPUD1 clone EPR9649 (cat#ab150424, Abcam), rat monoclonal anti-GRP94 clone SPM249 (cat#ab233979, Abcam, Cambridge, United Kingdom). We used the following polyclonal antibodies: rabbit anti-LC3 (cat#2775S, Cell Signaling Technology), rabbit anti-PERK (cat#P0074, Sigma-Aldrich), rabbit anti-STARD3 (cat#ab3478, Abcam, Cambridge, United Kingdom), goat anti-CATHEPSIN-D (cat#AF1014, R&D Systems, Minneapolis, MN, United States), rabbit anti-TFEB (cat#4240, Cell Signaling Technologies), rabbit anti-HERPUD1 (cat#BML-PW9705, ENZO Life Sciences, Farmingdale, NY, United States). Horseradish peroxidase-conjugated secondary antibodies were purchased from Jackson ImmunoResearch Laboratories (West Grove, PA, United States), Alexa fluorophore-conjugated secondary antibodies were purchased from Thermo Fisher Scientific.

Mass Spectrometry Based Proteomics and Statistical Analysis

Human H4 neuroglioma cells stably expressing shLuc and shATG5 were grown in Dulbecco's modified Eagle's medium lacking all amino acids except L-lysine and L-arginine, which were replaced with either unlabelled amino-acids (Lys0 and Arg0) or stable isotopic forms 13C6 15N2-lysine (Lys8) and 13C6 15N4-arginine (Arg10) (Cambridge Isotope Laboratories). The medium was supplemented with 10% dialyzed FBS using previous published methods (Golebiowski

et al., 2009; Yin et al., 2012). Two separate cultures of each shLuc and shATG5 cells were grown in light amino acids (Lys0 + Arg0) or heavy amino acids (Lys8 + Arg10) over nine replication cycles to achieve over 96% incorporation and similar cell counts per culture. Both cell cultures were divided in two, and cells were grown under control conditions in DMEM + 10% FBS or starvation in EBSS media for 4 h so that each cell type grown with each label were treated with both conditions (8 cultures in total). Cells were washed and lysed in 1.2 × LDS sample buffer with reducing agent, obtaining crude cell extracts at approximately 1 mg/ml. To allow all experimental conditions to be compared with one another a light reference mix was obtained by combining all four light amino acid conditions in a 1:1:1:1 ratio by volume. This was then mixed 1:1 ratio (v:v) with each heavy amino acid extract. The same comparisons were made in reverse by combining all heavy amino acid samples into a reference mix and combining this 1:1 (v:v) with each of the four individual light amino acid conditions. All eight mixes were fractionated by SDS-PAGE and stained gels were cut into three slices per lane before tryptic peptides were extracted. The resultant 24 samples of dried down peptides were resuspended in 35 μ l 0.1% TFA 0.5% acetic acid. Peptide samples were analyzed by LC-MS/MS twice; the first using 9 μ l peptide sample run over a 90 min peptide fractionation gradient, and the second using 18 μ l peptide sample run over a 240 min fractionation gradient. Peptides were analyzed using a Q exactive mass spectrometer (Thermo Scientific) coupled to an EASY-nLC 1,000 liquid chromatography system (Thermo Scientific), using an EASY-Spray ion source (Thermo Scientific), running a 75 μ m × 500 mm EASY-Spray column at 45°C. A top 10 data-dependent method was applied. Full scan spectra (m/z 300–1,800) were acquired with resolution R = 70,000 at m/z 200 (after accumulation to a target value of 1,000,000 with maximum injection time of 20 ms). The most intense ions were fragmented by HCD and measured with a resolution of R = 17,500 at m/z 200 (target value of 500,000 maximum injection time of 60 ms) and intensity threshold of 2.1×10^4 . Peptide match was set to "preferred", a 40 s dynamic exclusion list was applied, and ions were ignored if they had an assigned charge state of 1, 8 or >8. All 48 data files were analyzed simultaneously in MaxQuant (v1.5.2.8) using default parameters excepting the selection of SILAC labels, activation of 'requantify' and 'match between runs', using a uniprot 'HUMAN' proteome database (downloaded 24/02/2015- 73920 entries) as search space. Raw files derived from the same mix were grouped under the 'Experiment' heading as Mix01-Mix08. Raw files were given MaxQuant experimental design 'fraction' numbers such that spectra derived from the same HPLC gradient and from the equivalent gel slices across different lanes would be matched, as well as one sliced either side. 4,395 protein groups were listed as informed in the **Supplementary File S1**, proteinGroups.txt sheet. This list was edited to leave 3,911 protein groups by removing decoy proteins, protein listed as potential contaminants, proteins identified only by modified peptides, and proteins without a H/L ratio reported for any comparison (see **Supplementary File S1**, accepted sheet). The average of normalized forward and reverse ratios of starvation/control were

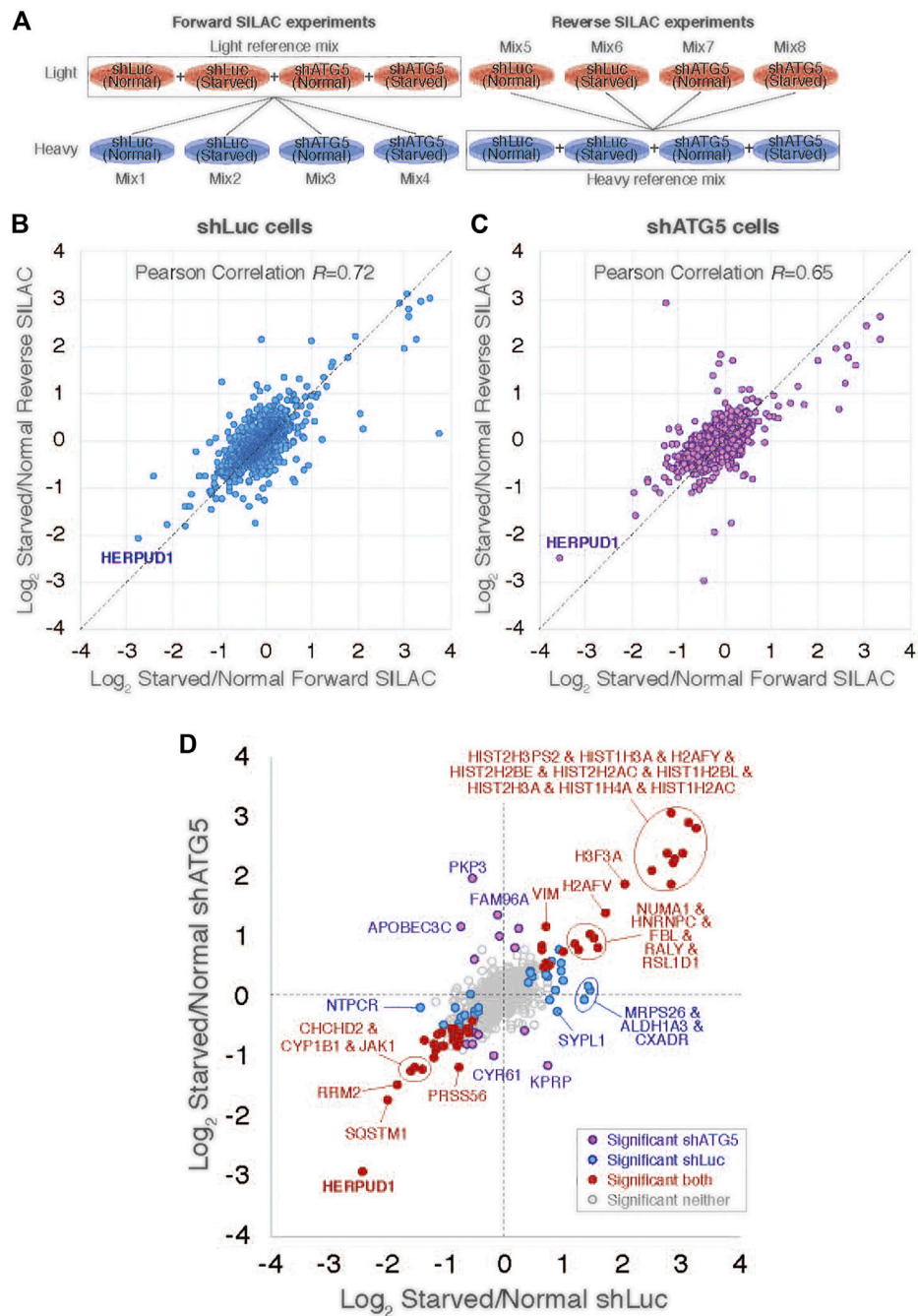


FIGURE 1 | SILAC-based proteomic study reveals HERPUD1 as a possible modulator of autophagy. **(A)** Design of the SILAC experiment to monitor changes of the cellular proteome of H4 cells during starvation and shRNA-mediated knockdown of ATG5 (shATG5) or shRNA against the luciferase gene (shLuc). 'Reference' mixes of all cell extracts were prepared for light and heavy conditions for 'forward' and 'reverse' SILAC experiments and were mixed 1:1 with individual cell extracts, giving a total of eight mixes. **(B,C)** Scatter plot comparing 'Forward' and 'Reverse' Log_2 Starvation/Normal ratio data for cells shLuc **(B)** and shATG5 **(C)**. **(D)** Comparison of average Log_2 Starvation/Normal ratios in shLuc (x-axis) and shATG5 (y-axis). Protein outliers under either or both knockdown conditions are colored as indicated.

carried forward for statistical analysis, but only for those with H/L ratios reported for both. These values along with average log_{10} protein intensities were used in Perseus to calculate Significance B

values to identify statistical outliers ($\text{SigB} < 0.001$) for the three ratios. Data for these shortlisted proteins are summarized in **Supplementary File S1**, shortlisted sheet. Data is available via

ProteomeXchange with identifier PXD024486. Reviewer account details: Username: reviewer pxd024486@ebi.ac.uk Password: ibjQUyjo.

Plasmids and Site-Directed Mutagenesis

For all HERPUD1 constructs generated in this study, previously described cDNAs encoding either the full-length or the Δ UBL deletion mutant human HERPUD1, both with a C-terminal FLAG-tag, were used as templates (Sai et al., 2003). pCI-HERPUD1-FLAG and pCI- Δ UBL-FLAG were digested with EcoRI and NotI restriction enzymes to obtain an insert, which was sub-cloned to a lentiviral pLVX-IRES-Puro vector (Takara Bio Inc., CA, United States) containing a puromycin resistance gene. The substitution S59D and S59A were introduced into the pLVX-IRES-FLAG-tagged HERPUD1 vector using the QuikChange II XL direct-mutagenesis kit (Stratagene, cat#200522) and the mutagenesis service of GenScript (Hong Kong, China).

Cell Culture and Generation of Stable Cell Lines

Maintenance of H4 human neuroglioma cells stably expressing either shRNAs against ATG5 or luciferase genes was performed as previously described (González et al., 2017). HeLa cells were obtained from the American Type Culture Collection (Manassas, VA, United States). HeLa-derived cell lines were cultured in Dulbecco's modified Eagle's medium (DMEM; Thermo Fisher Scientific) supplemented with 10% (vol/vol) heat-inactivated fetal bovine serum (FBS; Thermo Fisher Scientific), and 100 U/ml penicillin/100 mg/ml streptomycin (Thermo Fisher Scientific), in a 5% CO₂ atmosphere at 37°C. The generation of HeLa stable cell lines expressing all different variants of FLAG-tagged HERPUD1 cloned in the pLVX-IRES-Puro vector were generated by transfection with Lipofectamine 2000 (Invitrogen) according to manufacturer's instructions. After 24 h the cells were selected and maintained with 2 μ g/ml of puromycin.

Preparation of Protein Extracts, Electrophoresis, SDS-PAGE and Western Blot Analysis

Cells were washed with ice-cold phosphate buffered saline (PBS) and lysed in Radioimmunoprecipitation assay buffer (RIPA lysis buffer) [50 mM Tris-HCl, 150 mM NaCl, 5 mM EDTA, 1% NP-40, 1% sodium deoxycholate, 0.1% SDS, pH 7.4], supplemented with a cocktail of protease inhibitors [416 μ M 4-(2-Aminoethyl) benzenesulfonyl fluoride, 0.32 μ M Aprotinin, 16 μ M Bestatin, 5.6 μ M E-64, 8 μ M Leupeptin and 6 μ M Pepstatin A; Sigma-Aldrich] and phosphatase inhibitors (1 mM NaF, 0.3 mM Na₂P₂O₇ and 1 mM Na₃VO₄; Sigma-Aldrich). Cell lysates were collected and lysed for 30 min at 4°C in rotation. Then, extracts were sonicated with ultrasonic power three times on ice with pulses of 2–3 s at 40 mA using a tip sonicator system. Extracts were further centrifuged for 20 min at 13,000 \times g at 4°C. The supernatants were collected, and protein concentration was quantified using the BCA assay (ThermoFisher Scientific). The

protein extracts were denatured at 65°C for 5 min and analyzed using our previous described methods (González et al., 2017; Bustamante et al., 2020).

Transmission Electron Microscopy

HeLa cells were fixed for 16 h by immersion in 2.5% glutaraldehyde in 0.1 M cacodylate buffer (pH 7.0) at room temperature, and then washed three times with a cacodylate buffer for 2 h. Cells were post-fixed with 1% osmium tetroxide (OsO₄) for 2 h and washed three times with double distilled water. Then, the cells were treated with 1% aqueous uranyl for 90 min, and sequentially dehydrated through an acetone battery 50, 70, 95, and 100% for 20 min each. Cells were pre-embedded in epon/acetone 1:1 overnight and then in pure epon for 4 h. Finally, cells were embedded in fresh resin and polymerized in an oven at 60°C for 48 h. Ultrafine sections (80 nm) were obtained using an ultramicrotome Leica Ultracut R. The sections were incubated with 4% uranyl acetate in methanol for 2 min and lead citrate for 5 min. The grids were visualized using a Philips Tecnai 12 electron microscope (Eindhoven, Netherlands) at 80 kV. This work was performed in the Advanced Microscopy Facility of the Faculty of Biological Sciences at Pontificia Universidad Católica de Chile.

Fluorescence Microscopy, Data Acquisition, Quantification and High-Resolution Analysis

Cells grown on glass coverslips were washed with PBS-Ca²⁺/Mg²⁺ and then fixed, permeabilized and stained using our published protocols (Bustamante et al., 2020; Cavieres et al., 2020). The images were acquired using a TCS SP8 laser-scanning confocal microscope (Leica Microsystems, Wetzlar, Germany) equipped with a \times 63 oil immersion objective (1.4 NA), photomultipliers (PMT), hybrid detectors (HyD) system using 405 nm, 488 nm, 561 nm and 643 nm laser lines for excitation running the LASX Leica software. For image quantification, 16-bit (1024 \times 1024) images were acquired under identical settings avoiding signal saturation. Cell and nucleus area measurements were performed by using ICY software (Quantitative Image Analysis Unit, Institut Pasteur, <http://icy.bioimageanalysis.org/>). A pipeline was created to completely automate image analysis by using the following sequential plugins: active contours (cell segmentation), hk-means (threshold detection), wavelet spot detector (spot detection) and studio (colocalization). Total Fluorescence Integrated intensity measurement was performed by using ImageJ (FIJI) (Schindelin et al., 2012). The number of dots (lysosomes) was performed by using the LOG detector algorithm available on the TrackMate plugin (FIJI). For live cell imaging assays, HeLa cells were grown in glass bottom culture dishes (MatTek Corporation, Ashland, MA, United States) and labeled with the following Invitrogen probes: ER-Tracker™ Blue-White DPX (E12353), LysoTracker™ Red DND-99 (L7528, Invitrogen) and Magic-red (Immunochemistry Technologies, LLC) according to the manufacturer's protocol. Before image acquisition, culture medium was replaced with phenol red-free DMEM supplemented with HEPES (10 mM, pH 7.4), and images were

acquired with the $\times 63$ oil immersion objective (1.4 NA) of the TCS SP8 laser-scanning confocal microscope, running the Leica Application Suite LAS X software, coupled to a controlled temperature chamber (UNO-temp controller, OKOLAB) acquiring 16-bit images at 37°C (488 laser for excitation; HyD: 510–550 nm; $1,024 \times 1,024$ pixels; frame average 2). For volume analysis, z-stack (0.3 μm z-interval, 1024×1024 , 180 μm pixel size) images were quantified using 3D analysis plugin by using ICY software. Total fluorescence integrated intensity and dots number were measured using ImageJ. High Resolution Analysis: Colocalization analysis of ER/lysosomes contacts was performed using Huygens software (SVI, Netherlands). Briefly, images were acquired as described above but oversampling upon Nyquist parameters (Nyquist Calculator). Images were then deconvolved (CMLE blind deconvolution) and 3D rendered with Surface Render plugin. Colocalization volumes were quantified using the advanced particle analyzer and colocalization plugin. Only colocalization patches bigger than $0,5 \text{ mm}^3$ and smaller than 10 mm^3 were counted.

RNA Isolation and RT-PCR Analysis

Total RNA extraction from HeLa cells, oligo-dT and MMLV reverse transcriptase and quantitative reverse transcription PCR of the cDNA template (RT-PCR) was carried out as previously described (Bustamante et al., 2020). The specific primer pairs used for CYCLOPHILIN-A, CYCA (NM_001300981.2) and XBP1 (NM_001079539.2) were the following: CYCA-F TCG AGTTGTCCACAGTCAGC, CYCA-R TTCATCTGCACTGCC AAGAC, XBP1-F CGCTTGGGGATGGATGCCCTG and XBP1-R CCTGCACCTGCTGCGGACT.

Cell Viability Assays

Exponentially growing cells stably expressing either FLAG-tagged HERPUD1-WT or HERPUD1-S59D were trypsinized and seeded at 20,000 cells per well in 96-well microplates and allowed to attach for 6 h at 37°C and 5% CO_2 . Then, cells were incubated with CDDP in serial dilutions from 1 mM to 1 μM in 2% FBS medium and were incubated for 24 h at 37°C and 5% CO_2 . After drug incubation, the IC50 was obtained using the Sulforhodamine B (SRB) cell cytotoxicity assay (Blois et al., 2011). Briefly, cells were fixed (10% trichloroacetic acid, 4°C, 1 h), water washed, dried and stained (0.4% SRB v/v in 0.1% acetic acid, 1 h at RT), and then washed four times (1% acetic acid). Dissolved SRB (10 mM Tris-base, pH 10) was quantified (564 nm, Synergy HT BioTek reader). CDDP treatments were done in quadruplicate in at least three independent experiments. The IC50 values associated with the cytotoxic effects of CDDP were calculated using GraphPad Prism software (version 8.2; GraphPad Software, San Diego, CA, United States) using non-linear regression model and dose-response equations (log(inhibitor) vs. normalized response). After drug incubation, apoptotic cells were analyzed with the commercial kit Vybrant Apoptosis Pacific Blue-annexin V (cat#A35122, Invitrogen) using the protocol provided by the manufacturer. Briefly, cells stably expressing either FLAG-tagged HERPUD1-WT or HERPUD1-S59D were treated with 10 μM CDDP for 24 h. Cells were harvested and

centrifuged at $800 \times g$ for 5 min at room temperature and washed with cold PBS 1X. Cells were re-centrifuged, and the pellet resuspended in 100 μl annexin-binding buffer. Then, 5 μl of the annexin V conjugate was added to the cell suspension and incubated for 15 min at room temperature. After, 400 μl of annexin-binding buffer was added, gently mixed, and maintained on ice for later analysis in a BD FACSCanto II flow cytometer (Flow Cytometer Facility of Cell 4 Cell, Santiago, Chile), with a previous incubation with 3 μl of 7-Amino-Actinomycin D (7AAD) to exclude non-viable cells (included in the kit).

Densitometric Quantification and Statistical Analysis

The amount of immunoblot signal was estimated using Image J software version 1.48v (Wayne Rasband, NIH, <http://imagej.nih.gov>). For each condition, protein bands were quantified from at least three independent experiments in order to ensure adequate statistical power. Data analysis was performed using Microsoft Excel 2013 for Windows (Redmond, WA, United States) or GraphPad Prism 6. Results are represented in graphs depicting the mean \pm standard deviation. Statistical significance of data comparisons from two groups comparisons was determined with two-tailed unpaired Student's *t*-test for parametric data. Values of $p < 0.05$ (*), $p < 0.01$ (**), $p < 0.001$ (***) were regarded as statistically significant and are indicated in the figures.

RESULTS

HERPUD1 is a Regulator of Autophagy Under the Control of its UBL Domain

Previous reports have demonstrated a close interplay between autophagy and the Ubiquitin-Proteasome System (Bustamante et al., 2018), however, to date, few proteasomal substrates are known as modulators of autophagy (Jia and Bonifacino, 2019; Guarascio et al., 2020; Thayer et al., 2020). To search for potential novel candidates that could be downregulated by the proteasome in order to activate autophagy, we performed a SILAC-based proteomic study to quantitatively determine the proteome of H4 neuroglioma cells under basal and induced autophagy by EBSS starvation conditions. To eliminate all proteins downregulated because of autophagy activation, we compared the proteome of H4 cells where autophagy is inhibited by stable depletion of ATG5 by shRNA-mediated knockdown (shATG5) respect to control H4 cells expressing an shRNA against the luciferase gene (shLuc), both cell lines previously characterized (González et al., 2017; Tapia et al., 2019; **Figure 1A**). ATG5 protein is part of a complex with ATG12 and ATG16L that controls an essential step in the autophagosome formation (Walczak and Martens 2013). Silencing of ATG5 causes a strong inhibition in LC3B-positive autophagosomes, a phenotype also previously confirmed in our H4 cell lines (González et al., 2017). Among all the proteins downregulated by EBSS starvation, we found that in both H4 cell lines, shLuc (**Figure 1B**) and shATG5 (**Figure 1C**) the most significantly

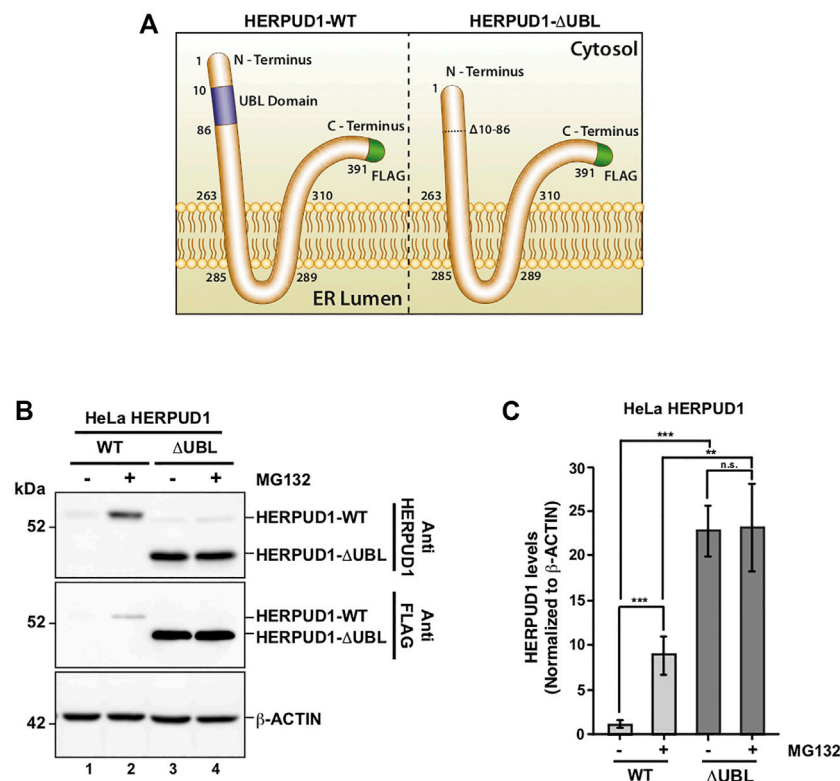


FIGURE 2 | Deletion of UBL domain increases HERPUD1 protein levels. **(A)** Schematic representation HERPUD1-WT (left image) and Δ UBL (right image) at the ER membrane, both FLAG-tagged at the carboxyl-terminus (shown in green). The Ubiquitin-Like domain (UBL, amino acids 10–86) are represented in purple. **(B)** HeLa cells stably expressing the WT or Δ UBL versions of HERPUD1 were not treated (lanes 1 and 3) or treated with 20 μ M of MG132 for 4 h (lanes 2 and 4). Detergent-soluble protein extracts were analyzed by western blot with anti-HERPUD1 and anti-FLAG antibodies. β -ACTIN was used as loading control. Image is representative of three independent experiments. Position of molecular mass markers is indicated on the left. **(C)** Densitometry quantification of HERPUD1 protein levels from images as those shown in B. Bars represent the mean \pm standard deviation of western blot signal normalized with β -ACTIN. Statistical analysis was performed using two-tailed unpaired Student's *t*-test ($n = 3$, n.s. not statistically significant, ** $p < 0.01$ and *** $p < 0.001$).

downregulated protein was HERPUD1, a protein originally identified as a homocysteine-inducible gene, that is also upregulated by endoplasmic reticulum (ER) stress (Kokame et al., 2000; Kokame et al., 2001). Importantly, HERPUD1 is an ER-stress membrane protein whose levels under non-stressful conditions are low due to proteasome degradation (Kokame et al., 2000; Sai et al., 2003). Indeed, pharmacological inhibition of the proteasome leads to a rapid increase of HERPUD1 levels (Sai et al., 2003; Miura et al., 2010). In addition to HERPUD1, we found several other proteins significantly down- or up-regulated by EBSS treatment (Figure 1D). However, while some proteins were down- or up-regulated by EBSS treatment in both, shLuc and shATG5 stable expressing cell lines (Figure 1D, red dots), many other hits were only down or up-regulated dependent on ATG5 protein expression (Figure 1D, purple dots). The complete list of proteins that responded significantly to EBSS treatment in both cell lines is shown in Supplementary Figure S1. Here, we focus on the characterization of HERPUD1, the hit with the highest score of downregulation in both cell lines, working with the hypothesis that its reduction by EBSS treatment could be indicative of its role as negative regulator of autophagy activity. Previous studies had shown that silencing HERPUD1 triggers the

autophagic flux (Quiroga et al., 2013). Therefore, in this study, and considering that HERPUD1 levels are increased under ER stress, we study the cellular consequences of HERPUD1 stability on autophagy function. HERPUD1 is an integral membrane protein with both termini facing the cytoplasm, with the ubiquitin-like domain (UBL) located in its N-terminus (Figure 2A; UBL: purple color, left side). Here, we cloned full-length HERPUD1 into the pLVX-IRES-Puro vector with a FLAG-tagged in its C-terminal end (Figure 2A; FLAG: green color) designed as HERPUD1-WT. In addition, we cloned a FLAG-tagged HERPUD1 version lacking the residues between Val¹⁰-Cys⁸⁶ designed as HERPUD1- Δ UBL (Figure 2A; right side), as previously reported (Sai et al., 2003). Further, we generated puromycin-resistant HeLa cells stably expressing either HERPUD1-WT or HERPUD1- Δ UBL, considering that previous characterization of HERPUD1 in HeLa cells was done only by transient transfection (Sai et al., 2003). Western blot analysis using either anti-HERPUD1 and anti-FLAG antibodies showed higher levels of HERPUD1- Δ UBL compared to HERPUD1-WT (Figure 2B, lane 1 and lane 3). In fact, we found a significant increase in the levels of HERPUD1- Δ UBL (22.83 ± 2.90) compared to HERPUD1-WT (1.00 ± 0.49)

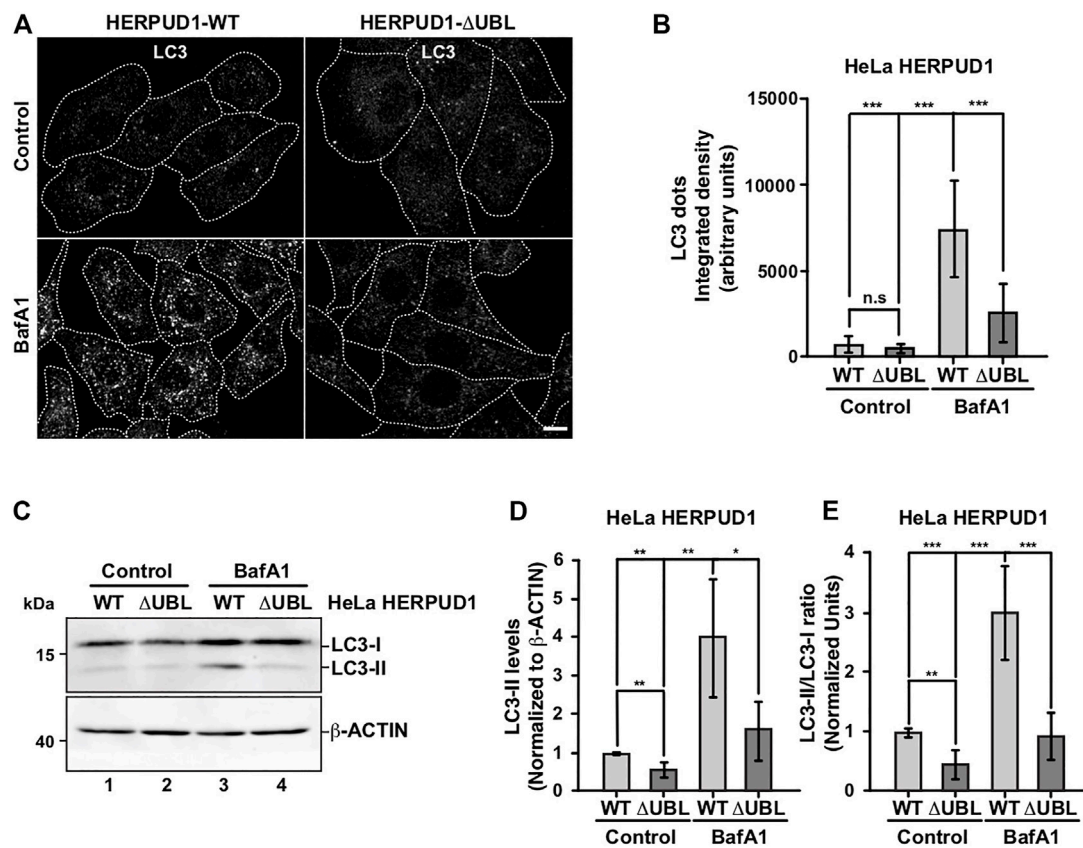


FIGURE 3 | The stabilization of HERPUD1 by its UBL deletion negatively regulates autophagy. **(A)** HeLa cells stably expressing HERPUD1-WT-FLAG or HERPUD1-ΔUBL-FLAG were grown in glass coverslips and were treated or not with 100 nM BafA1 for 4 h. Cells were fixed and incubated with an antibody to LC3 followed by incubation with Alexa-488-conjugated donkey anti-rabbit IgG. Stained cells were examined by confocal microscopy. Scale bar 10 μm. **(B)** Quantification of integrated density of LC3 puncta per cell under treatment with 100 nM BafA1 for 4 h. Bars represent the mean ± standard deviation ($n = 30$). **(C)** HeLa cells stably expressing HERPUD1-WT-FLAG or HERPUD1-ΔUBL-FLAG untreated (lanes 1 and 2) or treated with 100 nM BafA1 for 4 h (lanes 3 and 4). Detergent-soluble protein extracts were analyzed by western blot with a rabbit polyclonal antibody against LC3. Monoclonal antibody against β-ACTIN (clone BA3R) was used as loading control. Position of molecular mass markers is indicated on the left. **(D)** Densitometry quantification of LC3-II protein levels normalized with β-ACTIN. Bars represent the mean ± standard deviation. Statistical analysis was performed using two-tailed unpaired Student's t-test ($n = 3$ * $p < 0.05$, ** $p < 0.01$). **(E)** Densitometry quantification of LC3-I and LC3-II protein levels from images as those shown in C. Relative levels are expressed as the ratio of LC3-II to LC3-I. Bars represent the mean ± standard deviation. Statistical analysis was performed using two-tailed unpaired Student's t-test ($n = 3$ ** $p < 0.01$, *** $p < 0.001$).

under basal conditions (Figure 2C). The UBL is a domain that resembles ubiquitin in terms of their primary sequence and three-dimensional structure, considered a general interaction motif with the proteasome particularly with the 19S regulatory particle of the 26S proteasome (Hartmann-Petersen and Gordon, 2004a). Interestingly, it has been previously shown that deletion of UBL in HERPUD1 abolishes its proteasomal degradation (Sai et al., 2003). To confirm this, we treated the cells during 4 h with 20 μM MG132, a potent blocker of the proteasome activity (Tsubuki et al., 1996; Lee, 1998). As expected, we observed that this treatment caused an increase in the levels of overexpressed HERPUD1-WT (9.00 ± 2.90) in comparison to untreated cells (1.00 ± 0.49) (Figure 2B, lane 1 and 2) and Figure 2C. In contrast, HERPUD1-ΔUBL did not respond to this treatment, observing similar levels in the absence or presence of MG132 (22.83 ± 2.90 vs. 23.24 ± 4.89) (Figure 2B, lane 3 and 4) and Figure 2C, confirming previous findings (Sai et al., 2003). Together, these results confirmed HERPUD1-

ΔUBL is a tool to explore the effect of HERPUD1 stability on autophagy.

Therefore, we investigated the effect of HERPUD1-ΔUBL stable expression by analyzing the subcellular distribution of the microtubule-associated protein 1 light chain 3B (LC3B), a classical marker of autophagy, from here referred for simplicity as LC3 (Tanida et al., 2008). Immunofluorescence analysis of LC3 in cells expressing HERPUD1-WT and HERPUD1-ΔUBL showed basal autophagy represented by LC3-positive membrane dots that correspond to autophagosomes decorated with lipidated LC3 (LC3-II) observing no significant differences between cell lines (Figures 3A,B). Because autophagosomes are constantly forming autolysosomes through the fusion with acidic lysosomes for degradation, we tested the effect of BafA1, a drug that raises the lysosomal pH resulting in the perturbation of the autophagic flux (González et al., 2017). Upon BafA1 treatment we found HERPUD1-WT cells showed a significant increase in the interated density of LC3 dots fluorescence (7046.4 ± 3223.2)

LC3-II/LC3-I ratio in HERPUD1- Δ UBL cells treated with BafA1 (0.94 ± 0.37), respect control cells (3.01 ± 0.78) (**Figure 3E**). Importantly, similar findings were obtained under induced autophagy by EBSS starvation medium (**Supplementary Figure S2**). We observed that the LC3-II/LC3-I ratio in HERPUD1- Δ UBL cells in the presence of EBSS plus BafA1 was diminished with respect HERPUD1-WT cells (**Supplementary Figure S2A**, line 5 and 6 and **Supplementary Figure S2B**). Altogether, these findings strongly indicate that increased stability of HERPUD1 plays a negative effect on autophagy.

Increased Stability of HERPUD1 by the Deletion of its UBL Domain Triggers Remodeling of the ER in Stacked Tubular Structures Resembling Crystalloid ER-Like Structures in the Absence of ER Stress

Because previous reports have shown that defective autophagy leads to ER expansion (Ou et al., 1995; Jung et al., 2008) we investigated whether HERPUD1 stability could be linked with ER remodeling. In contrast to previous studies where only transient expression of HERPUD1- Δ UBL was characterized (Sai et al., 2003), we investigated the subcellular distribution of FLAG-tagged HERPUD1- Δ UBL but in stable HeLa cell lines, in comparison with its wild type version. Immunofluorescence analysis with an anti-FLAG antibody showed a stronger signal for HERPUD1 in the absence of its UBL domain (**Figure 4A**, FLAG, lower left panel) in comparison to HERPUD1-WT (**Figure 4A**, upper left panel). A similar result was also observed with an anti-HERPUD1 antibody (**Supplementary Figure S3A**). To unveil if this phenotype was affecting the ER in general, we analyzed by immunofluorescence the distribution of endogenous ER proteins markers. First, we tested endogenous CALNEXIN, an ER membrane resident protein that acts as a molecular chaperone of glycoproteins (Ou et al., 1995) and GRP94, an ER resident membrane protein of the Heat-Shock Protein (HSP) 90 family (Marzec et al., 2012). We found profound changes in the distribution of both proteins showing a similar pattern to anti-FLAG in HERPUD1- Δ UBL cells (**Figure 4A**, CALNEXIN and GRP94, lower panel), compared to HERPUD1-WT where a characteristic ER pattern is observed. Indeed, HERPUD1- Δ UBL shows a nice colocalization with CALNEXIN and GRP94 (**Figure 4A**, lower merge). In addition, and to exclude the possibility that this phenotype was specific to CALNEXIN and GRP94, we analyzed the ER pattern using an ER-tracker probe in live cells, observing clear changes in the morphology of the ER respect to HERPUD1-WT (**Supplementary Figure S3B**). We noticed that in comparison to HERPUD1- Δ UBL, HERPUD1-WT did not show a high colocalization with CALNEXIN and GRP94 (**Figure 4A**, upper merge), which can be explained by the low levels of HERPUD1-WT expression due to its constant degradation by the proteasome under basal conditions (Sai et al., 2003). In this regard, localization of HERPUD1 at the ER has been well documented (Kokame et al., 2000). Whereas HERPUD1- Δ UBL did not cause an increase in the levels of CALNEXIN and GRP94 measured by Western blot

analysis (**Supplementary Figure S3C y 3D**), we concluded that HERPUD1 stability by the deletion of its UBL domain causes an ER-like expansion phenomena that does not involve the increase in the levels of CALNEXIN and GRP94. HERPUD1 is known to be upregulated under ER stress, a condition reported to cause ER membrane expansion and remodeling to alleviate this condition (Schuck et al., 2009). Therefore, we studied whether HERPUD1- Δ UBL could be causing ER proliferation. To assess this, we performed immunofluorescence analysis with an anti-GRP94 antibody. Interestingly, we observed that HERPUD1- Δ UBL expressing cells present a large and dense ER network extending throughout the entire cytoplasm including the periphery of the cell, compared to the less extended ER network observed in HERPUD1-WT cells (**Figure 4B**, left and right panel). To gain a more comprehensive understanding of the ER differences between HERPUD1-WT and HERPUD1- Δ UBL expressing cells, we measured the ER volume using 3D images at high magnification taken with a z-interval of $0.3 \mu\text{m}$ followed by a z-stack maximum intensity projection. For visualization, we analyzed the distribution of GRP94 in the whole cell using a heat map gradient ranging from non-intensity (black color) to the higher intensity (red color) (**Figure 4B**, left and right panel). This analysis confirmed HERPUD1- Δ UBL increases the volume of the ER and the ER remodeling, compared to the expression of HERPUD1-WT. Indeed, quantitative analysis showed a significant increase in the ER volume with the expression of HERPUD1- Δ UBL (2361 ± 967), compared to HERPUD1-WT (1700 ± 689) (**Figure 4C**). The ER morphological changes observed by confocal microscopy prompted us to perform ultra-structural analysis by transmission electron microscopy (TEM). While cells expressing HERPUD1-WT showed the common ER cytoplasmic structures (**Figure 4D** left panel [ER]), unexpectedly HERPUD1- Δ UBL showed a high number of stacked tubular structures that resemble tubular ER structures that were oriented in a hexagonal spatial distribution (**Figure 4D** center panel [ER]). Others have referred to these structures as energetically stable structures formed by a remarkable proliferation of smooth ER, resembling crystalloid structures of ER (Chin et al., 1982; Anderson et al., 1983; Pathak et al., 1986; Borgese et al., 2006), which in appearance can be compared with “honeycomb like-structures” (**Figure 4D** center panel [ER]). Additionally, a higher magnification (**Figure 4D**, right panel), strongly indicates these structures resemble crystalloid structures with the absence of attached ribosome structures.

To gain insights whether the ER proliferation triggered by the expression of HERPUD1- Δ UBL was the result of an ER stress response, we studied X-box binding protein 1 (XBP1) as a reporter of ER stress and the unfolded protein response (UPR). First, we analyzed by RT-PCR the XBP1 mRNA processing, from the unspliced inactive XBP1 mRNA (uXBP1) form to the spliced active XBP1 mRNA (sXBP1) form (**Figure 5A**), which is considered a hallmark of the UPR response (Yoshida et al., 2001). RT-PCR analysis of mRNA from HeLa WT untreated cells showed a single band as expected (**Figure 5A**, lane 1). The same analysis including tunicamycin (Tun) (inhibitor of N-linked glycosylation (Heifetz et al., 1979) and thapsigargin (Tg) (blocker of ER

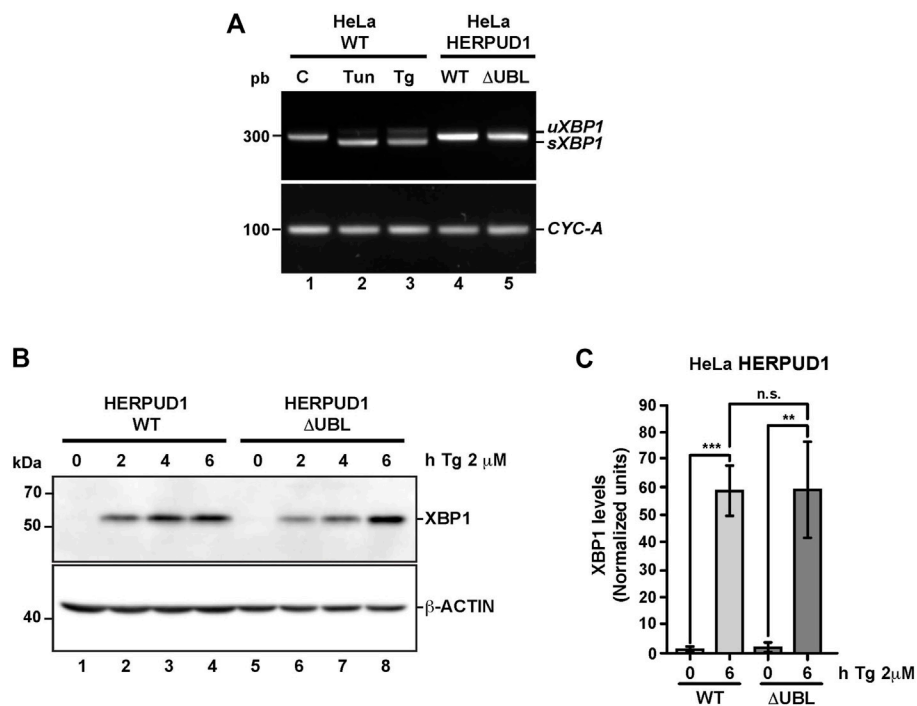


FIGURE 5 | The stability of HERPUD1 by the deletion of its UBL domain does not trigger endoplasmic reticulum stress. **(A)** Splicing of *XBP1* was analyzed by RT-PCR. Total RNAs were obtained from HeLa cells stably expressing HERPUD1-WT-FLAG or HERPUD1-ΔUBL-FLAG, additionally, total RNA was obtained from HeLa WT cells untreated or treated with 2 μM Thapsigargin (Tg) or 5 μg/ml Tunicamycin (Tun) for 4 h as a control of *XBP1* splicing. Then, cDNA was synthesized and mRNA expression of *XBP1* was analyzed using specific primers. (*uXBP1*: unspliced form, *sXBP1*: spliced form). CYCLOPHILIN-A (*CYC-A*) was used as an internal control. **(B)** HeLa cells stably expressing HERPUD1-WT-FLAG or HERPUD1-ΔUBL-FLAG were treated with 2 μM Thapsigargin (Tg) for different timepoints (0, 2, 4, and 6 h). Detergent-soluble protein extracts were analyzed by western blot with a monoclonal antibody against *XBP1*. Monoclonal antibody against β-ACTIN was used as loading control. Position of molecular mass markers is indicated on the left. **(C)** Densitometry quantification of *XBP1* protein levels from images as those shown in **B**. Bars represent the mean ± standard deviation. Statistical analysis was performed using two-tailed unpaired Student's *t*-test ($n = 3$ n.s. not statistically significant, $**p < 0.01$, $***p < 0.001$).

Ca²⁺ import (Thastrup et al., 1990)) as positive inducers of ER stress, produced the appearance of two bands in HeLa-WT cells, indicating the *sXBP1* form in response to ER stress (Figure 5A, lane 2 and 3). In contrast, a stable expression of either HERPUD1-WT or HERPUD1-ΔUBL showed no detection of *sXBP1*, observing only the expression of the *uXBP1* form (Figure 5A, lane 4 and 5), similar to untreated control HeLa WT untreated cells (Figure 5A, lane 1). Analysis of PCR bands relative to *CYCLOPHILIN A* (*CYC-A*) as a housekeeping control showed no difference between cells expressing either HERPUD1-WT or HERPUD1-ΔUBL proteins (Figure 5A, lane 4 and 5). Similar findings were observed by western blot analysis (Figure 5B). *sXBP1* is rapidly translated to a highly active transcription factor, known as *XBP1*, responsible for the upregulation of a variety of UPR genes (Yoshida et al., 2001). To examine the significance of the UBL domain of HERPUD1 in the response to ER stress induction, HERPUD1-WT cells and HERPUD1-ΔUBL cells were treated with 2 μM Tg for 2, 4, and 6 h and we performed western blot

analysis for *XBP1* detection. We observed *XBP1* protein was almost undetectable in both cell lines in the absence of a stressor (Figure 5B, lane 1 and 5). In contrast, we observed a robust induction of *XBP1* in both cell lines upon treatment for 2, 4, and 6 h with 2 μM Tg, observing similar *XBP1* expression levels after 6 h of treatment in both cell lines (Figure 5B, lane 4 and 8). Quantitative analysis confirmed this conclusion, observing no significant differences between HERPUD1 WT (58.99 ± 9.18) and HERPUD1-ΔUBL (59.59 ± 17.49) expressing cells (Figure 5C). In addition to *XBP1*, we tested by western blot analysis the ER resident transmembrane protein PERK, a kinase that undergoes hyperphosphorylation in response to ER stress shown as a shift in its mobility during SDS-polyacrylamide gel electrophoresis (Bertolotti et al., 2000). This kinase mediates the attenuation of the global translation by the phosphorylation of eIF2α (Bertolotti et al., 2000; Harding and Zhang, 2000). In contrast to its differential electrophoretic migration with Tun and Tg (Supplementary Figure S4, lane 2 and 3), no changes in

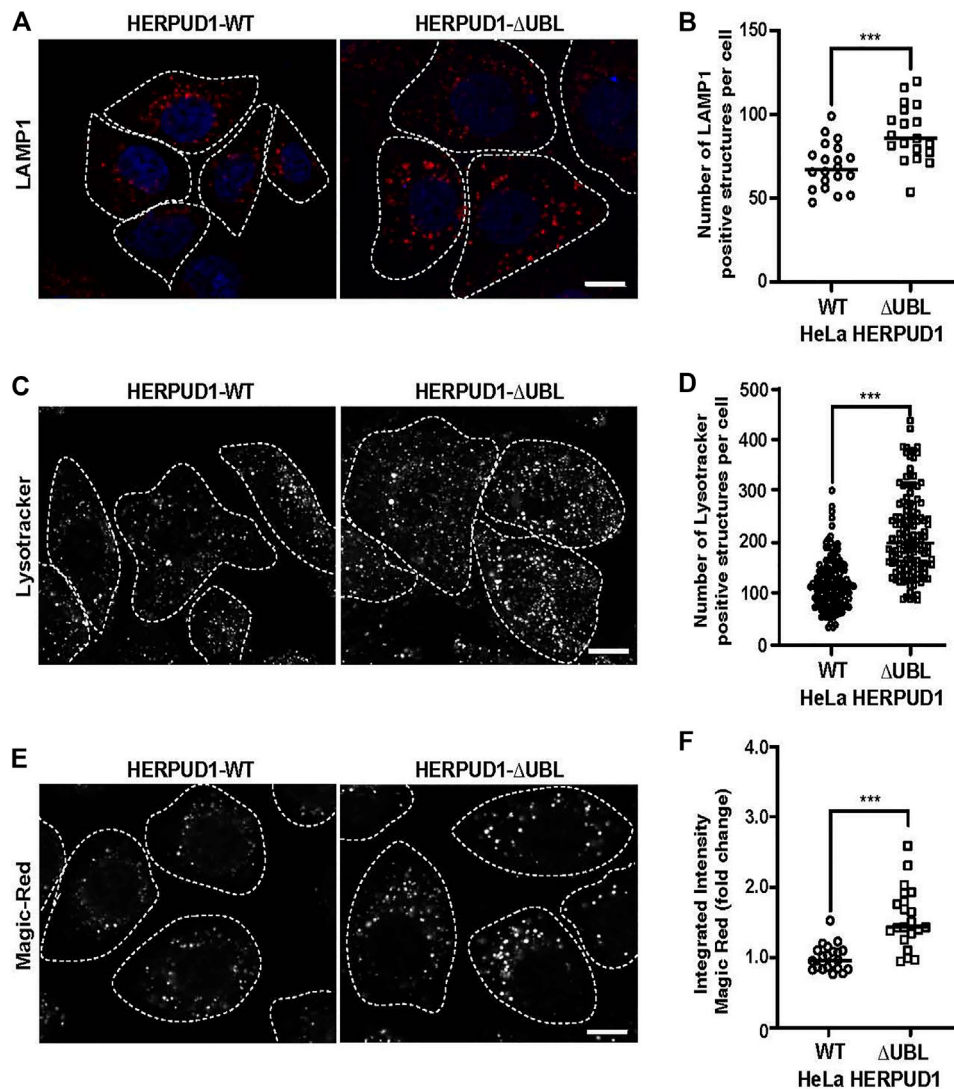


FIGURE 6 | Expression of HERPUD1- Δ UBL increases lysosomal number and function. **(A)** HeLa cells stably expressing HERPUD1-WT-FLAG or HERPUD1- Δ UBL-FLAG grown in glass coverslips were fixed, permeabilized and labeled with a mouse monoclonal antibody against LAMP1 followed by incubation with Alexa-594-conjugated donkey anti-mouse IgG, and DAPI for nuclei staining. Stained cells were examined by fluorescence microscopy. Images were acquired using a TCS SP8 laser-scanning confocal microscope. Scale bar 10 μ m. **(B)** Quantification of LAMP1 positive structures per cell. In the scatter plot each circle and square represents the average of positive LAMP1 dots per cell from a frame of HeLa HERPUD1-WT ($n = 559$) or HERPUD1- Δ UBL ($n = 700$) respectively. The quantified cells were from three independent experiments. **(C,E)** HeLa cells stably expressing HERPUD1-WT-FLAG or HERPUD1- Δ UBL-FLAG were grown in glass bottom culture dishes and labeled with **(C)** LysoTracker™ Red DND-99 or **(E)** Magic Red[®]. For live cell imaging analysis, culture medium was replaced with phenol red-free DMEM supplemented with HEPES (10 mM, pH 7.4) and images were acquired with TCS SP8 laser-scanning confocal microscope at 37°C. Scale bar 10 μ m. **(D)** Quantification of LysoTracker™ dots per cell. Open circles and open squares represent the average of fluorescence signals for each cell of HeLa HERPUD1-WT-FLAG ($n = 139$) or HERPUD1- Δ UBL-FLAG ($n = 138$) respectively. **(F)** Quantification of Magic Red[®] positive structures. In the scatter plot each circle and square represents the average of positive dots for Magic Red per cell from a frame of HeLa HERPUD1-WT-FLAG ($n = 1,279$) or HERPUD1- Δ UBL-FLAG ($n = 984$) respectively. The quantified cells were from three independent experiments. Statistical analysis was performed using two-tailed unpaired Student's *t*-test (** $p < 0.001$).

PERK migration were observed in HERPUD1-WT or HERPUD1- Δ UBL cells (**Supplementary Figure S4**, lane 4 and 5). Analysis of the activating transcription factor 4 (ATF4), a protein highly expressed upon UPR response

(Harding and Novoa, 2000) showed again no changes in ATF4 levels in either cell line (**Supplementary Figure S4**, lane 4 and 5). In contrast, a robust detection of ATF4 was found upon the addition of Tun and Tg (**Supplementary**

Figure S4, lane 2 and 3). Altogether, our findings strongly indicate that ER remodeling triggered by HERPUD1 stability is not the consequence of ER stress.

Increased HERPUD1 Stability by the Deletion of its UBL Domain Leads to a Remarkable Increase in Lysosomal Number and Function

ER proliferation that excludes ribosomes is able to regulate ER contacts with lysosomes (Friedman et al., 2013; Lee and Craig, 2020). Lysosomes are an important catabolic organelle of eukaryotic cells, containing a diverse repertoire of acidic hydrolases (luminal pH of 4.5–5.0) that can digest macromolecules such as sugars, lipids and proteins and even entire organelles (Xu and Ren, 2015). We asked whether expanded ER by increased HERPUD1 stability could have an impact on endolysosomal organelles. To visualize these compartments, HERPUD1-WT and HERPUD1- Δ UBL expressing HeLa cells were stained with an antibody against the endogenous lysosomal-associated membrane protein 1 (LAMP1), a membrane protein found on late endosomes and lysosomes (Griffiths et al., 1988). Unexpectedly, we observed a robust increase in LAMP1 positive structures located around the entire cytoplasm (**Figure 6A**). In agreement with this finding, quantification analysis showed a significant increase in the number of LAMP1 positive structures in HERPUD1- Δ UBL (88.72 ± 16.77) respect to control cells (69.03 ± 13.79) (**Figure 6B**). To determine if the increase in LAMP1 structures corresponded to lysosome organelles, we performed co-staining of LAMP1 with CATHEPSIN-D (CAT-D), a luminal hydrolytic lysosomal enzyme (Benes et al., 2008), observing several LAMP1 positive structures positive to CAT-D (**Supplementary Figure S5A**, lower merge). In addition, we noticed a significant increase in the integrated fluorescence intensity of CAT-D in HERPUD1- Δ UBL (1.47 ± 0.88), compared to HERPUD1-WT expressing cells (1.00 ± 0.20) (**Supplementary Figure S5B**). Considering this increase in CAT-D fluorescence we evaluated if HERPUD1- Δ UBL also impacts lysosomal activity, as assessed by measuring lysosomal acidity and activity in live cells. We first measured if HERPUD1 stability affects the range of lysosomal pH, using the pH-sensitive lysosomal dye LysoTracker Red, which accumulates and emits red fluorescence in acidic compartments with pH < 6.5 (De Duve and Christian, 1974; Chou et al., 2001). Then, we measured CATHEPSIN-B activity using the Magic Red assay (Boonacker et al., 2003). As shown in **Figure 6C**, expression of HERPUD1- Δ UBL causes a significant increase in the number of LysoTracker positive structures (211.95 ± 78.90), compared to control cells (117.85 ± 48.97) (**Figures 6C,D**). Similarly, we found an increase in the number of structures positive to Magic Red fluorescence (**Figure 6E**). This was confirmed by measuring the integrated fluorescence intensity, which revealed a significant increase of this parameter in HERPUD1- Δ UBL cells (1.56 ± 0.43), compared to control cells (1.00 ± 0.19) (**Figure 6F**). Altogether, these findings show that ER remodeling triggered by HERPUD1 increased stability is a potent strategy to promote lysosomal function.

The Phosphomimetic Mutant S59D in the UBL Domain Promotes HERPUD1 Stability Mimicking the Effects of UBL Deletion on the ER and Autophagy

Further, we searched for a mechanism that could mimic the phenotype observed by the deletion of UBL on HERPUD1. As shown by the analysis with PyMOL molecular graphics system (**Supplementary Figure S6A**), the UBL domain of HERPUD1 (PDB 1WGD; green color) resembles UBIQUITIN (PDB 2MSG; purple color) in terms of their three-dimensional structure. UBIQUITIN as well as UBL domains are known targets of phosphorylation under cellular stress (Kondapalli et al., 2012; Swaney et al., 2015; Sauvé et al., 2018). In fact, oxidative stress promotes phosphorylation of UBIQUITIN at Ser65 causing the accumulation of ubiquitylated proteins due to a reduction in global protein turnover rates (Koyano et al., 2014; Swaney et al., 2015). In the same line, it is known that the UBL domain on PARKIN is phosphorylated by PINK1 and is responsible for the activation of its E3 ubiquitin-ligase activity (Sauvé et al., 2018), both essential players of mitochondria quality control by mitophagy (Jin and Youle 2012). Thereby, we searched for Ser residues as possible candidates of phosphorylation in the UBL domain of HERPUD1 using the KinasePhos2.0 web tool. Five residues were predicted in position Ser16, Ser27, Ser33, Ser59, and Ser90 (**Supplementary Figure S6B**, Ser residues in red color). For all these five Ser residues, we generated phosphoinert (substitutions to alanine) and phosphomimetic (substitutions to aspartic acid) mutant versions. Stably transfected HeLa cells were generated for each mutant. Among all mutations tested, the substitution S59D, but not the S59A, showed the strongest increase in HERPUD1 signal, as is shown by immunofluorescence with an anti-FLAG antibody (**Figures 7A,B**). Importantly, we found that the phosphomimetic S59D mutant presents an ER pattern very similar to HERPUD1- Δ UBL cells, confirmed by co-staining with GRP94 (**Figure 7A**, right panel merge). Moreover, to evaluate the specificity of the ER remodeling phenotype in HERPUD1- Δ UBL and HERPUD1-S59D expressing cells, we performed silencing of HERPUD1 with a specific siRNA. In both cell lines we observed a robust rescue of the ER pattern positive to CALNEXIN, compared to the siControl (**Supplementary Figure S7A**). Silencing of HERPUD1- Δ UBL and HERPUD1-S59D with the siRNA was confirmed by western blot (**Supplementary Figure S7B**). Also, no changes with the phosphoinert S59A mutant were observed, showing a similar phenotype than HERPUD1-WT (**Figures 7A,B**). Thus, further characterization included the comparison between HERPUD1-WT and HERPUD1-S59D. In this regard, under basal conditions western blot analysis using anti-HERPUD1 and anti-FLAG antibodies showed higher levels of HERPUD1-S59D (40.09 ± 5.31) compared to either HERPUD1-WT (1.00 ± 0.53) or HERPUD1-S59A (2.88 ± 1.76) (**Figure 7C**, lane 5 compared to lane 1 and 3 and **Figure 7D**). We also measured the levels of these versions upon treatment for 4 h with 20 mM MG132, which is a proteasomal inhibitor, known to abolish HERPUD1 proteasomal degradation (Yan et al., 2014). As expected, MG132 treatment caused a significant increase in HERPUD1-WT (16.55 ± 7.13) (**Figure 7C**, lane 1 compared to lane 2 and **Figure 7D**). A similar result was obtained with HERPUD1-S59A (20.36 ± 9.65) (**Figure 7C**, lane 3

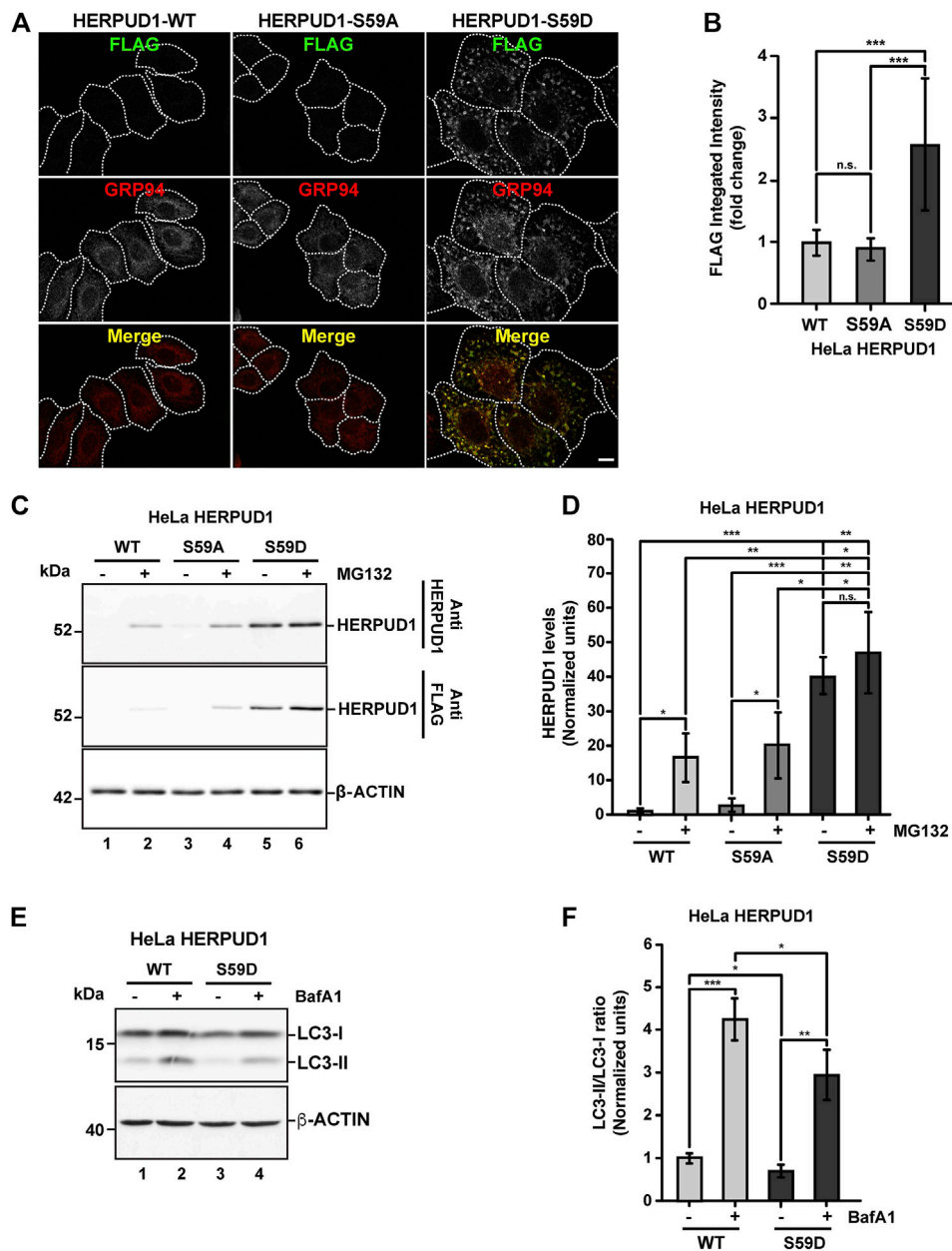
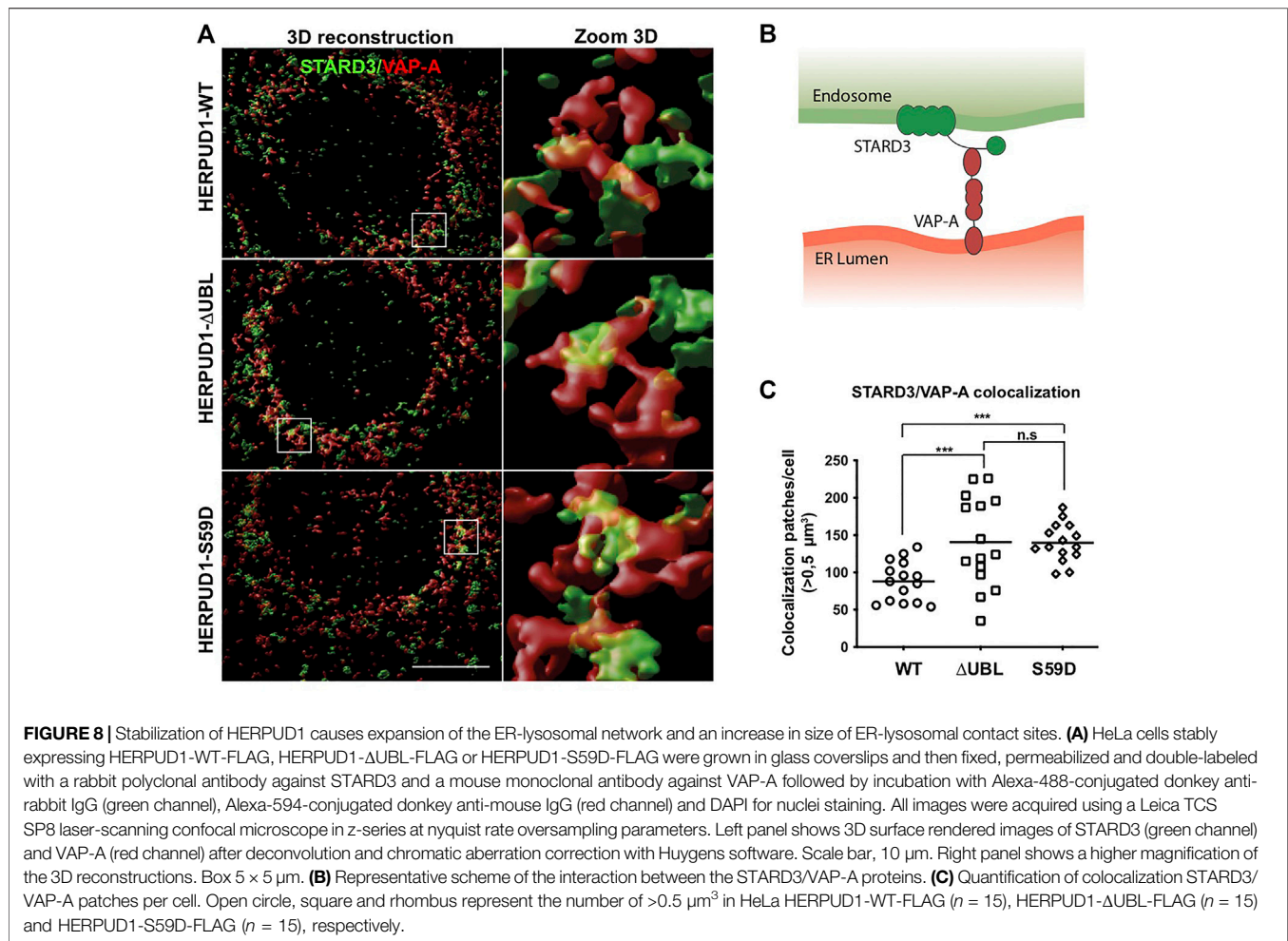


FIGURE 7 | Stabilization of HERPUD1 by S59D mutation alters the ER morphology and decreases autophagy. **(A)** HeLa cells stably expressing HERPUD1-WT-FLAG, HERPUD1-S59A-FLAG or HERPUD1-S59D-FLAG were grown in glass coverslips, fixed, permeabilized, and double-labeled with mouse monoclonal antibody against FLAG and with a rat monoclonal antibody against GRP94 followed by incubation with Alexa-488-conjugated donkey anti-rabbit IgG (green channel) and Alexa-594-conjugated donkey anti-rat IgG (red channel). Images were acquired using a TCS SP8 laser-scanning confocal microscope. The third image on each column is the merge of green and red channels; yellow indicates colocalization of red and green channels. Scale bar: 10 μ m. **(B)** Quantification of fluorescence FLAG signal from indicated cells. **(C)** HeLa cells stably expressing HERPUD1-WT-FLAG, HERPUD1-S59A-FLAG or HERPUD1-S59D-FLAG were treated or not with 10 μ M of MG132 for 4 h. Detergent-soluble protein extracts were analyzed by western blot with anti-HERPUD1 and anti-FLAG antibodies. β -ACTIN was used as a loading control. Position of molecular mass markers is indicated on the left. **(D)** Densitometry quantification of HERPUD1 western blot signal from images as those shown in **C**. Bars represent the mean \pm standard deviation. **(E)** HeLa cells stably expressing HERPUD1-WT-FLAG or HERPUD1-S59D-FLAG untreated (lanes 1 and 3) or treated with 100 nM BafA1 for 4 h (lanes 2 and 4). Detergent-soluble protein extracts were analyzed by western blot with a rabbit polyclonal antibody to LC3B. Monoclonal antibody against β -ACTIN was used as a loading control. Position of molecular mass markers is indicated on the left. **(F)** Densitometry quantification of LC3-I and LC3-II protein levels from images as those shown in **E**. Relative levels are expressed as the ratio of LC3-II to LC3-I from images as those shown in **E**. Bars represent the mean \pm standard deviation. Statistical analysis was performed using two-tailed unpaired Student's *t*-test ($n = 3$ n.s. not statistically significant, * $p < 0.05$, ** $p < 0.01$, *** $p < 0.001$).



compared to lane 4 and **Figure 7D**). In contrast, we observed non-significant differences in the levels of HERPUD1-S59D in the absence (40.09 ± 5.31) or presence of MG132 (47.17 ± 11.74) (**Figure 7C**, lane 5 and 6 and **Figure 7D**). Further, and based on the negative impact of HERPUD1 stability on autophagy by the deletion of its UBL domain, we next investigated if the stability of HERPUD1-S59D could have a similar outcome. Biochemically, we found that HERPUD1-S59D cells have a significant reduction in the LC3-II/LC3-I ratio (0.66 ± 0.02), in comparison to HERPUD1-WT (1.00 ± 0.18) (**Figures 7E,F**). This result was corroborated by immunofluorescence analysis of LC3 in the absence or presence of BafA1 showing that HERPUD1-S59D cells present a lesser number of autophagosomes, compared to HERPUD1-WT (**Supplementary Figure S8**). Moreover, in agreement with previous reports indicating that a reduction in autophagy enhances ER expansion and cell size (Khaminets et al., 2015; Miettinen and Mikael, 2015), we noticed that HERPUD1-S59D cells were significantly larger in size (2.52 ± 0.98), compared to HERPUD1-WT (1.00 ± 0.4) and HERPUD1-S59A cells (0.88 ± 0.29) (**Figure 7A** and **Supplementary Figure S9A**). Importantly, cell size quantification showed HERPUD1- Δ UBL were also larger in size (1.36 ± 0.64) than HERPUD1-WT (1.00 ± 0.4), but smaller than HERPUD1-S59D (2.52 ± 0.98) (**Supplementary Figure S9A**). In addition, because nuclei size remains proportional to the cell size in a

wide range of genetic backgrounds and growth conditions (Huber and Gerace, 2007), we studied the nuclei size in all cell lines. Surprisingly, nuclei size in HERPUD1-S59D cells were significantly larger (1.74 ± 0.72) in comparison to all tested cell lines; HERPUD1-WT (1.00 ± 0.49), HERPUD1-S59A (1.12 ± 0.47) and HERPUD1- Δ UBL (1.11 ± 0.52) (**Supplementary Figure S9B**). Altogether, our findings support the idea that HERPUD1 increased stability might play an important function in cellular plasticity by commanding a program that controls ER remodeling with impact in cell and nuclei size. The results with the phosphomimetic version of HERPUD1 opens the alternative of a program activated under the control of phosphorylation.

The Phosphomimetic HERPUD1-S59D Mutant Promotes ER-Lysosomal Network With Impact in Stress Cell Survival

Because of the increase in the number of functional lysosomes under the expression of HERPUD1- Δ UBL, we investigated if HERPUD1-S59D expressing cells could have a similar output. First, we performed immunofluorescence of LAMP1, observing a significant increase in the number of LAMP1 positive structures in HERPUD1-S59D cells (135.28 ± 21.32), in comparison to

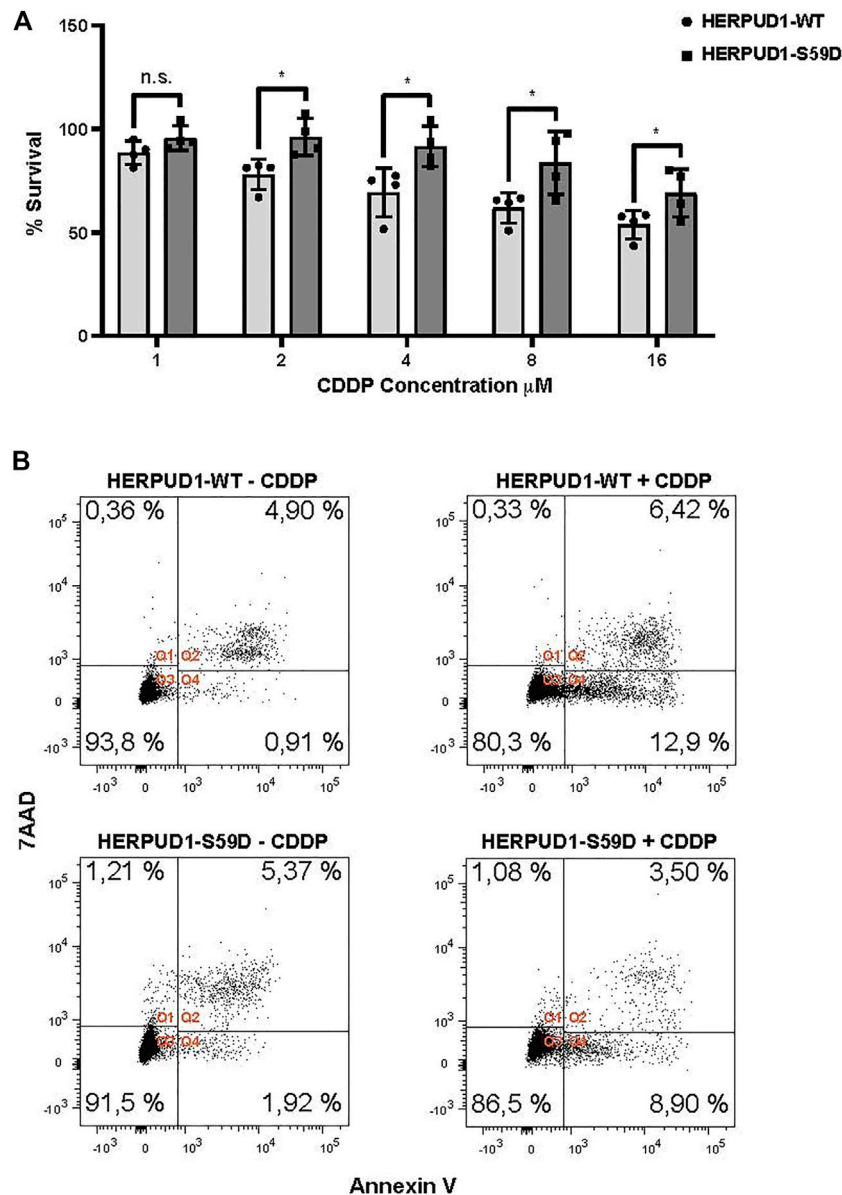


FIGURE 9 | Stabilization of HERPUD1 by S59D mutation decreases cell death mediated by CDDP. **(A)** HeLa cells stably expressing HERPUD1-WT-FLAG or HERPUD1-S59D-FLAG were treated with different concentrations of cisplatin (CDDP) and then a SRB assay was performed. The absorbance values of each point were normalized to control cells (without treatment) and transformed to a percentage. Experiments were performed at least three times, and the results are expressed as mean \pm standard deviation. Statistical analysis was performed using two-tailed unpaired Student's *t*-test ($n = 4$ n.s. not statistically significant and $*p < 0.05$) **(B)** HeLa cells stably expressing HERPUD1-WT-FLAG or HERPUD1-S59D-FLAG were treated or not with CDDP 10 μ M for 24 h. Afterwards, cells were collected by trypsinization and stained with Annexin V-Pacific Blue and 7AAD. Scatter plots representing the different quadrants are labeled as Q1 (necrotic cells), Q2 (viable cells), Q3 (dead cells) and Q4 (apoptotic cells). The graph shows the percentage of cells present in each quadrant.

HERPUD1-WT (69.03 ± 13.79) and HERPUD1-S59A (58.42 ± 14.55) (**Supplementary Figures S10A,B**). Next, analysis with LysoTracker in HERPUD1-S59D cells (183.35 ± 60.05), in comparison to HERPUD1-WT (118.18 ± 51.00) and HERPUD1-S59A (86.13 ± 41.46) confirmed HERPUD1-S59D cells have a significant increase in the number of lysosomes per cell (**Supplementary Figures S10C,D**). Similar results were obtained with Magic Red where the quantification showed an increase of almost twice the integrated intensity of Magic Red in

HERPUD1-S59D cells (2.25 ± 0.32) in comparison with HERPUD1-WT (1.00 ± 0.15) and HERPUD1-S59A (1.02 ± 0.24) (**Supplementary Figures S10E,F**). The integrated intensity analysis demonstrated the increase in lysosomal function is not a result of larger cell size suggesting the activation of an alternative mechanism that needs to be further investigated.

One important aspect of cellular plasticity is the establishment of a network between the ER and the lysosomes that helps in the

constant adaptation to particular cellular needs. In this regard, it is known that the ER forms membrane-contact sites (MCSs) with lysosomes (Valm and Alex, 2017), acting as a potent spatiotemporal organizer of endolysosomal biology (Neeffjes et al., 2017). We hypothesized that ER-lysosomal network remodeling should be accompanied by the appearance of MCSs between these two organelles. Therefore, we studied in HERPUD1-WT, HERPUD1- Δ UBL and HERPUD1-S59D cells the spatial distribution of the STARD3 endo-lysosomal cholesterol-binding protein (Alpy et al., 2001) with VAP-A, an ER membrane protein (Skehel et al., 2000), known to form a novel molecular tether between endo-lysosomes and the ER referred as MCSs (Alpy et al., 2013), in a high-resolution scale. By three-dimensional (3D) reconstruction imaging we observed that expression of HERPUD1- Δ UBL and HERPUD1-S59D caused larger patches of colocalization between STARD3/VAP-A (**Figure 8A**, left panel white boxes). A higher zoom 3D magnification of these white boxes is indicated in **Figure 8A**, right panel. A representative scheme of the interaction between the STARD3/VAP-A proteins is indicated in **Figure 8B**. Quantification analysis confirmed a significant increase in the number of colocalization patches $>0.5 \mu\text{m}^3$ per cell in HERPUD1- Δ UBL and HERPUD1-S59D expressing cells, compared to HERPUD1-WT (**Figure 8C**). Altogether, our findings strongly suggest that HERPUD1 stability at the ER compartment not only promotes the remodeling of the lysosomal network but also the size area of MCSs between these two organelles.

ER expansion has been known for decades as a trigger for crystalloid ER (Chin et al., 1982) and ER whorls (Feldman et al., 1981; Schuck et al., 2009), however only recent studies have proposed this phenomenon could be part of a program necessary to overcome ER stress with impact in stress cell survival (Schuck et al., 2009; Xu et al., 2021). Moreover, taking in consideration that HERPUD1 stability triggers ER expansion, ER-lysosomal network and MCSs between these two organelles, a protein known to be upregulated under ER stress, we studied the effect of HERPUD1 stability in the cell viability of HeLa cells in response to cisplatin (CDDP). CDDP is the most frequently used chemotherapeutic agent for the treatment of some types of cancers, including cervical cancer in accordance with the model of HeLa cells (Dasari and Bernard Tchounwou, 2014). In addition, it is known that alleviation of ER stress attenuates CDDP-induced apoptosis (Wu et al., 2018). Thus, we investigated the resistance to drug-induced cytotoxicity of HERPUD1-WT and HERPUD1-S59D cells in response to varying doses of CDDP for 24 h with the Sulforhodamine B (SRB) assay. We found a significant increase in the resistance of HERPUD1-S59D cells in comparison with HERPUD1-WT at 2, 4, 8, and 16 μM of CDDP (**Figure 9A**). We corroborated this result measuring apoptosis of these cells in the absence or presence of 10 μM CDDP for 24 h by flow cytometry using Annexin-V staining method. In agreement with the SRB assay, we observed HERPUD1-S59D cells showed less apoptosis compared to HERPUD1-WT cells in response to CDDP treatment (**Figure 9B**). These results strongly indicate HERPUD1 stability helps to overcome cisplatin-induced

cytotoxicity. In this regard, we propose that this differential response could be mediated by the expansion of the ER/lysosomal network, an aspect that should be investigated in other cancer cell models.

DISCUSSION

Post-translational events allow cells to respond swiftly to stress conditions with consequences in their proteome composition. Autophagy and the UPS are two closely related pathways that adjust their functions in response to cellular demands in order to maintain cellular homeostasis (Korolchuk et al., 2010). During starvation overall protein degradation rises by activation of both autophagy and the UPS (Mizushima et al., 2011; VerPlank et al., 2019). Indeed, before up-regulation of autophagy, efficient synthesis of new proteins is sustained by degradation of preexisting proteins by the proteasome, which shows that the proteasome also plays a crucial role in cell survival after nutritional stress (Vabulas and Ulrich Hartl, 2005). In agreement with this, it is known that the proteasome activity transits from a latent to an activated state (Asano et al., 2015; Collins and Goldberg, 2020). However, if UPS activation upon starvation mediates the degradation of specific proteins that could slow-down autophagy is unknown. Downregulation of HERPUD1 upon nutrient starvation in ATG5-depleted cells opens that alternative. In this regard, it has been previously proposed that HERPUD1 depletion up-regulates autophagy (Quiroga et al., 2013) and the degradation of cytosolic protein aggregates (Miura et al., 2010). These findings support the idea that basal levels of HERPUD1 could act as a break in the activation of basal autophagy.

Interestingly, another protein that was also robustly downregulated upon starvation in Atg5 KD cells was p62/SQSTM1. Been an autophagy receptor this protein could be also participating in endosomal microautophagy (Mejlvang et al., 2018), pathway that could be more activate with the lack of Atg5. Atg5^{-/-} mice remain healthy until the perinatal period, therefore it is accepted that cells activate alternative mechanisms to compensate the lack of Atg5 (Yoshii et al., 2016). In agreement with this hypothesis, p62/SQSTM1 KO mice show an increase in the ER content in the liver (Yang et al., 2016). Further studies will help to clarify unconventional roles of p62/SQSTM1.

Under ER stress, HERPUD1 is upregulated even faster than ER chaperones (Kokame et al., 2000; Bergmann et al., 2018), where it participates in Endoplasmic Reticulum-Associated Degradation (ERAD) (Schulze et al., 2005). HERPUD1 facilitates the assembly of the HRD1 complex, also known as the retrotranslocon, key in the retrotranslocation of unfolded proteins from the ER to the cytosol for proteasomal degradation upon demand (Leitman et al., 2014; Schulz et al., 2017). However, the function of HERPUD1 in the absence of ER stress is less understood. Here, we propose HERPUD1 acts as a negative regulator of autophagy controlled by its proteasome dependent stability, a mechanism that could operate in the absence of ER stress under the control of phosphorylation of its UBL domain.

One interesting aspect of HERPUD1 is the UBL domain present in its N-terminus region. In general, UBL-containing proteins share the ability to interact with the 19S regulatory particle of the 26S proteasome promoting its activation (Hartmann-Petersen and Gordon, 2004b; Yu and Matouschek, 2017; Collins and Goldberg, 2020). The UBL domain itself can stimulate multiple proteasome activities in a similar fashion to ubiquitin chains (Kim et al., 2018; Collins and Goldberg, 2020). However, unlike ubiquitin and its homologous (e.g., SUMO and Nedd8), UBL-containing proteins cannot be conjugated to other proteins. The human genome encodes over 60 UBL-containing proteins, where 15 of them have been studied in their ability to bind and regulate proteasome activity (Collins and Goldberg, 2020). HERPUD1 is one member of this group, however its role as a positive modulator of the proteasomal activity remains uncharacterized. Moreover, because UBL-containing proteins can stimulate proteasome activity (Kim et al., 2018; Collins and Goldberg, 2020), it would be interesting to explore the effect of HERPUD1- Δ UBL and HERPUD1-S59D on the activity of the proteasome under normal and starvation conditions.

In addition, recent findings show UBL-containing proteins can also play a regulatory role in autophagy, such as USP14 (Kim et al., 2018), NUB1 (Guarascio et al., 2020), Elongin B (Antonoli et al., 2016), UHRF1 (Shi et al., 2020), OASL (Toledo Pinto et al., 2018), BAT3 (Sebti et al., 2014) and UBQLN (Rothenberg et al., 2010; Şentürk et al., 2019; Yang and Klionsky 2020). Our findings show that the stabilization of HERPUD1 by removing its UBL domain causes a reduction in LC3-II/LC3-I ratio, which positions HERPUD1 as a member of this growing list of UBL-containing proteins that function as regulators of autophagy. However, how HERPUD1 stability mediates the reduction in LC3-II/LC3-I ratio needs further studies. One aspect to be explored is the finding that HERPUD1 interacts with UBQLN (Kim et al., 2008). UBQLN is a cytosolic protein, that in addition to HERPUD1, interacts with LC3 and ubiquitinated cargos in autophagosomes (Rothenberg et al., 2010). Furthermore, it is known that silencing UBQLN leads to a reduction in the lipidation of LC3-I to LC3-II that correlates with a diminished number of autophagosomes (Rothenberg et al., 2010). Because UBQLN binds HERPUD1 independently of its UBL domain (Kim et al., 2008), it is possible that an increase in HERPUD1 stability at the ER could mediate the sequestration of UBQLN in this compartment affecting its function in other membranes such as autophagosomes (Rothenberg et al., 2010). In this regard, it has been previously proposed that recruitment of UBQLN to the ER by HERPUD1 could bring the proteasome and the ubiquitinated substrates to specific microdomains of the ER, which could hypothetically be the step that promotes the ERAD pathway (Kim et al., 2008). Because our results show that HERPUD1 stability maintain the ER-lysosomal network, additional work is needed to determine if HERPUD1:UBQLN interaction could play a role in the delivery of substrates to the ER-to-lysosomes-associated degradation (ERLAD) (Fregno et al., 2018; Fregno and Molinari 2019), considering the increase in the lysosomal degradation function. As HERPUD1-S59D mimics the effect on HERPUD1

stability we propose that recruitment of UBQLN at the ER is controlled by phosphorylation of HERPUD1.

Ubiquitin and UBL domains are targets of phosphorylation (Kondapalli et al., 2012; Koyano et al., 2014; Wauer et al., 2015). The best-known example is the phosphorylation of the UBL domain of the ubiquitin ligase PARKIN by the Ser/Thr kinase PINK1 on Ser65 (Kondapalli et al., 2012; Koyano et al., 2014). This post-translational modification orchestrates its enzymatic E3 ligase activity (Aguirre et al., 2017), participating in the ubiquitination of mitochondrial proteins during mitophagy. Here, we propose that phosphorylation of the UBL domain in HERPUD1 must affect its noncovalent binding to the proteasome explaining its stability increase, as occurs with HERPUD1- Δ UBL. Further studies are needed to define the physiological triggers of HERPUD1 phosphorylation, and the kinase involved.

This study is the first report indicating HERPUD1 stability mediates ER expansion but not as a consequence of ER stress. In this regard, it is well known that the ER expands to alleviate ER stress (Schuck et al., 2009). However, the ER expansion phenomenon is not always homeostatic. ER expansion requires an adequate supply of membrane lipids although the mechanisms that govern ER biogenesis are yet unclear. For example, the ER expands several folds when B lymphocytes differentiate into antibody-secreting plasma cells (Wiest et al., 1990), when hepatocytes increase its P450 detoxification system (Feldman et al., 1981), in response to Epidermal Growth Factor (EGF) (Caldieri et al., 2017) and statins (Chin et al., 1982). Interestingly, lipid synthesis activation causes expansion of the ER and resistance to ER stress even in cells lacking the UPR, highlighting the physiological importance of ER membrane biogenesis in homeostasis. Because ER adjust its size and shape according to need interacting with several other organelles (Schuck et al., 2009), it has been proposed ER size can impact other organelles allowing rapid transfer of ions and newly synthesized lipids, associated to the shape and distribution of the ER (Chan and Marshall, 2010). However, how cells control cell size is still an enigma. Nevertheless, because cell size controls flux across membranes, metabolism, biosynthetic capacity, and nutrient exchange, among others, (Chan and Marshall, 2010), our findings open the possibility that stabilized HERPUD1 could play an important role in cell physiology, a mechanism that could be related with mTOR pathway and its downstream targets (Fingar et al., 2022).

A future challenge will be to sort out the connection between HERPUD1 and lipid synthesis, a link recently suggested by genomics (Van Der Laan and Sander, 2018).

In this regard, an interesting observation to be considered is that HERPUD1 increased stability mimics the effect of statins in reference to the appearance of a crystalloid ER (Chin et al., 1982). Statins are cholesterol reducing agents acting as blockers of the cholesterol biosynthesis by the inhibition of 3-hydroxy-3-methylglutaryl coenzyme A (HMG-CoA) reductase. Interestingly, statins possess beneficial effects in a variety of human diseases. Importantly, a growing number of studies refer to statins as ER stress reducing agents (Mollazadeh et al., 2018; Zhang et al., 2018), modulators of autophagy (Ashrafzadeh et al., 2020) and inducers of lysosomal biogenesis (Zhang et al.,

2020). However, if statins promote those effects by a mechanism related with HERPUD1 stability is unknown.

ER expansion by HERPUD1 stability is correlated with a slow-down in autophagy. In agreement with this, it is known that the knockdown of the two major autophagy regulators, ATG5 and BECN1, likewise trigger ER expansion (Khaminets et al., 2015). Moreover, a similar ER expansion is also observed by ER-phagy inhibition, a selective form of autophagy responsible for the degradation of excess ER (Khaminets et al., 2015; Grumati et al., 2018). However, studies investigating if the UPR is activated or not in response to inhibition of autophagosomal biogenesis or ER-Phagy dysfunction are still lacking. While the opposite effect has been reported, observing that excessive ER-Phagy results in activation of the UPR response (Liao et al., 2019).

Our findings also indicate that ER expansion by HERPUD1 stability is accompanied by an increase in the number of functional lysosomes. Because several studies have indicated that UBL-containing proteins cause a positive modulation of the UPS system we can speculate that HERPUD1- Δ UBL and HERPUD1-S59D could have a negative impact in the proteasome activity. Disturbances in the UPS and autophagy function are known to be compensated by lysosome biogenesis (Jackson and Hewitt 2016). In addition, we have already discussed the possibility that HERPUD1 stability could trigger the recruitment of UBQLN to the ER. Interestingly, it has been recently discovered that UBQLN plays a crucial role in the maintenance of the acidic pH of lysosomes and in a closed interplay with the ER (Şentürk et al., 2019; Yang and Klionsky, 2020). Further work is needed to determine if HERPUD1:UBQLN interaction could play a role at this level. Furthermore, based on recent findings (Toulmay and Prinz, 2011; Henne, 2017), it is necessary to explore if MCSs between ER and lysosomes could play a role in the transfer of lipids to lysosomes to compensate for the massive expansion of the ER under HERPUD1 stability by degradation.

Together, our findings highlight novel insights into the possible role of HERPUD1 as a regulator of autophagy and its participation in the maintenance of the ER structure. Moreover, our results suggest that HERPUD1 stabilization promotes the lysosomal function which could promote ER-lysosome intercommunication even in conditions where the UPR is not activated. The mechanism behind this regulation remains to be elucidated, specially the UBL phosphorylation-dependent stabilization of HERPUD1 and its effect on the pathways discussed above. Furthermore, if this regulation has a role in cell pathological conditions it should be analyzed in future studies.

REFERENCES

- Aguirre, J. D., Dunkerley, K. M., Mercier, P., and Shaw, G. S. (2017). Structure of Phosphorylated UBL Domain and Insights into PINK1-Orchestrated Parkin Activation. *Proc. Natl. Acad. Sci. USA* 114 (2), 298–303. doi:10.1073/pnas.1613040114
- Alpy, F., Rousseau, A., Schwab, Y., Legueux, F., Stoll, I., Wendling, C., et al. (2013). STARD3 or STARD3NL and VAP Form a Novel Molecular Tether between

DATA AVAILABILITY STATEMENT

The datasets presented in this study can be found in online repositories. The names of the repository/repositories and accession number(s) can be found below: ProteomeXchange with identifier PXD024486.

AUTHOR CONTRIBUTIONS

Design of experiments: GV, OC, EA-M, SH, CC-T, LH, AEG, MHT, HAB, CR, JC, MV-G, RTH, AR-F, VAC, PVB. Development of experiments: GV, OC, EA-M, CC-T, LH, AEG, MHT, HAB, MV-G, AR-F, VAC. Writing: GV, OC, EA-M, SH, MHT, CR, MV-G, AR-F, VAC, PVB.

FUNDING

This research was funded by Fondo Nacional de Desarrollo Científico y Tecnológico of Chile (FONDECYT; <http://www.conicyt.cl/fondecyt>) 1190928 to MV-G, No. 1211261 to PVB and No. 11150532 to AR-F; Associative Investigation Program (PIA; <https://www.conicyt.cl/pia>) including No. No. ACT-172066 to PVB; Financiamiento Basal No. ANID/BASAL/ACE210009 to PVB; No. ANID/BASAL/FB210008 to PVB Academy Insertion Program (PAI; <http://www.conicyt.cl/pai>) No. 79150075 to AR-F; Fondo de Equipamiento Científico y Tecnológico of Chile (FONDEQUIP; <http://www.conicyt.cl/fondequip>) No. EQM150118 to PVB; Cooperation International Programme (CONICYT-RCUK; <https://www.conicyt.cl/pci>) No. DPI20140068 to PVB.

ACKNOWLEDGMENTS

We thank the generous donation of pCI-HERPUD1-Flag and pCI-HERPUD1- Δ UBL-Flag by Doctor Koichi Kokame from National Cerebral and Cardiovascular Center, Japan. We also thank Zanlungo for the generous donation of the anti-STARD3 commercial antibody. Additionally, we thank Lavandero and Quiroga for the critical discussion of the manuscript.

SUPPLEMENTARY MATERIAL

The Supplementary Material for this article can be found online at: <https://www.frontiersin.org/articles/10.3389/fcell.2022.743287/full#supplementary-material>

Late Endosomes and the ER. *J. Cel Sci* 126 (Pt 23), 5500–5512. doi:10.1242/jcs.139295

- Alpy, F., Stoeckel, M.-E., Dierich, A., Escola, J.-M., Wendling, C., Chenard, M.-P., et al. (2001). The Steroidogenic Acute Regulatory Protein Homolog MLN64, a Late Endosomal Cholesterol-Binding Protein. *J. Biol. Chem.* 276 (6), 4261–4269. doi:10.1074/jbc.m006279200

- Anderson, R. G. W., Orci, L., and Brown, M. S. (1983). Ultrastructural Analysis of Crystalloid Endoplasmic Reticulum in UT-1 Cells and its Disappearance in Response to Cholesterol. *J. Cel Sci.* 63 (1), 1. doi:10.1242/jcs.63.1.1

- Antonioli, M., Albiero, F., Piacentini, M., and Fimia, G. M. (2016). Temporal Regulation of Autophagy Response by the CULLIN 4-AMBRA1-CULLIN 5 Axis. *Mol. Cell Oncol* 3 (5), e1008304. doi:10.1080/23723556.2015.1008304
- Asano, S., Fukuda, Y., Beck, F., Aufderheide, A., Förster, F., Danev, R., et al. (2015). A Molecular Census of 26 S Proteasomes in Intact Neurons. *Science* 347 (6220), 439–442. doi:10.1126/science.1261197
- Ashrafzadeh, M., Ahmadi, Z., Farkhondeh, T., and Samarghandian, S. (2020). Modulatory Effects of Statins on the Autophagy: A Therapeutic Perspective. *J. Cell Physiol* 235 (4), 3157–3168. doi:10.1002/jcp.29227
- Benes, P., Vetricka, V., and Fusek, M. (2008). Cathepsin D-Many Functions of One Aspartic Protease. *Crit. Rev. Oncology/Hematology* 68 (1), 12–28. doi:10.1016/j.critrevonc.2008.02.008
- Bergmann, T. J., Fregno, I., Fumagalli, F., Rinaldi, A., Bertoni, F., Boersema, P. J., et al. (2018). Chemical Stresses Fail to Mimic the Unfolded Protein Response Resulting from Luminal Load with Unfolded Polypeptides. *J. Biol. Chem.* 293 (15), 5600–5612. doi:10.1074/jbc.ra117.001484
- Bertolotti, A., Zhang, Y., Hendershot, L. M., Harding, H. P., and Ron, D. (2000). Dynamic Interaction of BiP and ER Stress Transducers in the Unfolded-Protein Response. *Nat. Cell Biol* 2 (6), 326–332. doi:10.1038/35014014
- Blois, J., Smith, A., and Josephson, L. (2011). The Slow Cell Death Response when Screening Chemotherapeutic Agents. *Cancer Chemother. Pharmacol.* 68 (3), 795–803. doi:10.1007/s00280-010-1549-9
- Boonacker, E., Elferink, S., Bardai, A., Wormmeester, J., and Van Noorden, C. J. F. (2003). Rapid Assay to Detect Possible Natural Substrates of Proteases in Living Cells. *BioTechniques* 35 (4), 766–774. doi:10.2144/03354st07
- Borgese, N., Francolini, M., and Snapp, E. (2006). Endoplasmic Reticulum Architecture: Structures in Flux. *Curr. Opin. Cell Biol.* 18 (4), 358–364. doi:10.1016/j.ccb.2006.06.008
- Bustamante, H. A., González, A. E., Cerda-Troncoso, C., Shaughnessy, R., Otth, C., Soza, A., et al. (2018). Interplay between the Autophagy-Lysosomal Pathway and the Ubiquitin-Proteasome System: A Target for Therapeutic Development in Alzheimer's Disease. *Front Cell Neurosci* 12, 126. doi:10.3389/fncel.2018.00126
- Bustamante, H. A., Cereceda, K., González, A. E., Valenzuela, G. E., Cheuquemilla, Y., Hernández, S., et al. (2020). The Proteasomal Deubiquitinating Enzyme PSMD14 Regulates Macroautophagy by Controlling Golgi-To-ER Retrograde Transport. *Cells* 9 (3), 777. doi:10.3390/cells9030777
- Caldieri, G., Barbieri, E., Nappo, G., Raimondi, A., Bonora, M., Conte, A., et al. (2017). Reticulon 3-Dependent ER-PM Contact Sites Control EGFR Nonclathrin Endocytosis. *Science* 356 (6338), 617–624. doi:10.1126/science.aah6152
- Camuzard, O., Santucci-Darmanin, S., Carle, G. F., and Pierrefite-Carle, V. (2020). Autophagy in the Crosstalk between Tumor and Microenvironment. *Cancer Lett.* 490, 143–153. doi:10.1016/j.canlet.2020.06.015
- Cavieres, V. A., Cerda-Troncoso, C., Rivera-Dicther, A., Castro, R. I., Luchsinger, C., Santibañez, N., et al. (2020). Human Golgi Phosphoprotein 3 Is an Effector of RAB1A and RAB1B. *PLoS ONE* 15 (8 August), e0237514. doi:10.1371/journal.pone.0237514
- Chan, Y.-H. M., and Marshall, W. F. (2010). Scaling Properties of Cell and Organelle Size. *Organogenesis* 6 (2), 88–96. doi:10.4161/org.6.2.11464
- Chin, D. J., Luskey, K. L., Anderson, R. G., Faust, J. R., Goldstein, J. L., and Brown, M. S. (1982). Appearance of Crystalloid Endoplasmic Reticulum in Compactin-Resistant Chinese Hamster Cells with a 500-Fold Increase in 3-Hydroxy-3-Methylglutaryl-Coenzyme A Reductase. *Proc. Natl. Acad. Sci. U S A.* 79 (4 I), 1185–1189. doi:10.1073/pnas.79.4.1185
- Chou, K.-M., Paul Krapcho, A., and Hacker, M. P. (2001). Impact of the Basic Amine on the Biological Activity and Intracellular Distribution of an Azanthrapyrazole: BBR 342244 Abbreviations: MDR, Multidrug Resistance; NHS-ASA, N-Hydroxysuccinimidyl-4-Azidosalicylic Acid; SRB, Sulforhodamine B; and P-Gp, P-Glycoprotein. *Biochem. Pharmacol.* 62 (10), 1337–1343. doi:10.1016/s0006-2952(01)00797-3
- Collins, G. A., and Goldberg, A. L. (2020). Proteins Containing Ubiquitin-like (Ubl) Domains Not Only Bind to 26S Proteasomes but Also Induce Their Activation. *Proc. Natl. Acad. Sci. USA* 117 (9), 4664–4674. doi:10.1073/pnas.1915534117
- Dasari, S., and Bernard Tchounwou, P. (2014). Cisplatin in Cancer Therapy: Molecular Mechanisms of Action. *Eur. J. Pharmacol.* 740, 364–378. doi:10.1016/j.ejphar.2014.07.025
- De Duve, C., Poole, T. B., Trouet, A., Tulkens, P., and Van Hoof, F. (1974). Commentary. Lysosomotropic Agents. *Biochem. Pharmacol.* 23 (18), 2495–2531. doi:10.1016/0006-2952(74)90174-9
- Demishtein, A., Fraiberg, M., Berko, D., Tirosh, B., Elazar, Z., and Navon, A. (2017). SQSTM1/P62-Mediated Autophagy Compensates for Loss of Proteasome Polyubiquitin Recruiting Capacity. *Autophagy* 13 (10), 1697–1708. doi:10.1080/15548627.2017.1356549
- Feldman, D., Swarn, R. L., and Becker, J. (1981). *Ultrastructural Study of Rat Liver and Liver Neoplasms after Long-Term Treatment with Phenobarbital*. London, United Kingdom: Cancer Research 41 (6), 2151–2162.
- Fingar, D. C., Salama, S., Tsou, C., Harlow, E., and Blenis, J. (2002). Mammalian Cell Size Is Controlled by mTOR and its Downstream Targets S6K1 and 4EBP1/eIF4E. *Genes Dev.* 16 (12), 1472–1487. doi:10.1101/gad.995802
- Fregno, I., et al. (2018). ER to Lysosome Associated Degradation of Proteasome Resistant ATZ Polymers Occurs via Receptor Mediated Vesicular Transport. *EMBO J.* 37 (17). doi:10.15252/embo.201899259
- Fregno, I., and Molinari, M. (2019). Proteasomal and Lysosomal Clearance of Faulty Secretory Proteins: ER-Associated Degradation (ERAD) and ER-To-Lysosome-Associated Degradation (ERLAD) Pathways. *Crit. Rev. Biochem. Mol. Biol.* 54 (2), 153–163. doi:10.1080/10409238.2019.1610351
- Friedman, J. R., DiBenedetto, J. R., West, M., Rowland, A. A., and Voeltz, G. K. (2013). Endoplasmic Reticulum-Endosome Contact Increases as Endosomes Traffic and Mature. *MBoC* 24 (7), 1030–1040. doi:10.1091/mbc.e12-10-0733
- Golebiowski, F., Matic, I., Tatham, M. H., Cole, C., Yin, Y., Nakamura, A., et al. (2009). System-Wide Changes to Sumo Modifications in Response to Heat Shock. *Sci. Signal.* 2 (72), ra24. doi:10.1126/scisignal.2000282
- González, A. E., Muñoz, V. C., Cavieres, V. A., Bustamante, H. A., Cornejo, V. H., Januário, Y. C., et al. (2017). Autophagosomes Cooperate in the Degradation of Intracellular C-Terminal Fragments of the Amyloid Precursor Protein via the MVB/Lysosomal Pathway. *FASEB J.* 31 (6), 2446–2459. doi:10.1096/fj.201600713R
- Griffiths, G., Hoflack, B., Simons, K., Mellman, I., and Kornfeld, S. (1988). The Mannose 6-Phosphate Receptor and the Biogenesis of Lysosomes. *Cell* 52 (3), 329–341. doi:10.1016/s0092-8674(88)80026-6
- Grumati, P., Dikic, I., and Stolz, A. (2018). ER-phagy at a Glance. *J. Cell Sci* 131 (17). doi:10.1242/jcs.217364
- Guarascio, R., Salih, D., Yasvoina, M., Edwards, F. A., Cheetham, M. E., and van der Spuy, J. (2020). Negative Regulator of Ubiquitin-like Protein 1 Modulates the Autophagy-Lysosomal Pathway via P62 to Facilitate the Extracellular Release of Tau Following Proteasome Impairment. *Hum. Mol. Genet.* 29 (1), 80–96. doi:10.1093/hmg/ddz255
- Harding, H. P., Novoa, I., Zhang, Y., Zeng, H., Wek, R., Schapira, M., et al. (2000). Regulated Translation Initiation Controls Stress-Induced Gene Expression in Mammalian Cells. *Mol. Cell* 6 (5), 1099–1108. doi:10.1016/s1097-2765(00)00108-8
- Harding, H. P., Zhang, Y., Bertolotti, A., Zeng, H., and Ron, D. (2000). Perk Is Essential for Translational Regulation and Cell Survival during the Unfolded Protein Response. *Mol. Cell* 5 (5), 897–904. doi:10.1016/s1097-2765(00)80330-5
- Hartmann-Petersen, R., and Gordon, C. (2004a). Integral UBL Domain Proteins: A Family of Proteasome Interacting Proteins. *Semin. Cell Dev. Biol.* 15 (2), 247–259. doi:10.1016/j.semcdb.2003.12.006
- Hartmann-Petersen, R., and Gordon, C. (2004b). Ubiquitin-Proteasome System. *Cell Mol. Life Sci.* 61 (13). doi:10.1007/s00018-004-4132-x
- Heifetz, A., Keenan, R. W., and Elbein, A. D. (1979). Mechanism of Action of Tunicamycin on the UDP-GlcNAc:dolichyl-Phosphate GlcNAc-1-Phosphate Transferase. *Biochemistry* 18 (11), 2186–2192. doi:10.1021/bi00578a008
- Henne, W. M. (2017). Discovery and Roles of ER-Endolysosomal Contact Sites in Disease. *Adv. Exp. Med. Biol.* 997, 135–147. doi:10.1007/978-981-10-4567-7
- Huber, M. D., and Gerace, L. (2007). The Size-Wise Nucleus: Nuclear Volume Control in Eukaryotes. *J. Cell Biol.* 179 (4), 583–584. doi:10.1083/jcb.200710156
- Jackson, M. P., and Hewitt, E. W. (2016). Cellular Proteostasis: Degradation of Misfolded Proteins by Lysosomes. *Essays Biochem.* 60 (2), 173–180. doi:10.1042/ebc20160005
- Jia, R., and Bonifacino, J. S. (2019). Negative Regulation of Autophagy by UBA6-BIRC6-Mediated Ubiquitination of LC3. *Elife* 8. doi:10.7554/eLife.50034
- Jin, S. M., and Youle, R. J. (2012). PINK1- and Parkin-Mediated Mitophagy at a Glance. *J. Cell Sci.* 125 (4), 795–799. doi:10.1242/jcs.093849

- Jung, H. S., Chung, K. W., Won Kim, J., Kim, J., Komatsu, M., Tanaka, K., et al. (2008). Loss of Autophagy Diminishes Pancreatic β Cell Mass and Function with Resultant Hyperglycemia. *Cel Metab.* 8 (4), 318–324. doi:10.1016/j.cmet.2008.08.013
- Khaminets, A., Behl, C., and Dikic, I. (2016). Ubiquitin-Dependent and Independent Signals in Selective Autophagy. *Trends Cel Biol.* 26 (1), 6–16. doi:10.1016/j.tcb.2015.08.010
- Khaminets, A., Heinrich, T., Mari, M., Grumati, P., Huebner, A. K., Akutsu, M., et al. (2015). Regulation of Endoplasmic Reticulum Turnover by Selective Autophagy. *Nature* 522 (7556), 354–358. doi:10.1038/nature14498
- Kim, E., Park, S., Lee, J. H., Mun, J. Y., Choi, W. H., Yun, Y., et al. (2018). Dual Function of USP14 Deubiquitinase in Cellular Proteasomal Activity and Autophagic Flux. *Cel Rep.* 24 (3), 732–743. doi:10.1016/j.celrep.2018.06.058
- Kim, H. T., and Goldberg, A. L. (2018). UBL Domain of Usp14 and Other Proteins Stimulates Proteasome Activities and Protein Degradation in Cells. *Proc. Natl. Acad. Sci. USA* 115 (50), E11642–E11650. doi:10.1073/pnas.1808731115
- Kim, T.-Y., Kim, E., Yoon, S. K., and Yoon, J.-B., (2008). Herp Enhances ER-Associated Protein Degradation by Recruiting Ubiquitins. *Biochem. Biophysical Res. Commun.* 369 (2), 741–746. doi:10.1016/j.bbrc.2008.02.086
- Kokame, K., Agarwala, K. L., Kato, H., and Miyata, T. (2000). Herp, a New Ubiquitin-like Membrane Protein Induced by Endoplasmic Reticulum Stress. *J. Biol. Chem.* 275 (42), 32846–32853. doi:10.1074/jbc.m002063200
- Kokame, K., Kato, H., and Miyata, T. (2001). Identification of ERSE-II, a New Cis-Acting Element Responsible for the ATF6-dependent Mammalian Unfolded Protein Response. *J. Biol. Chem.* 276 (12), 9199–9205. doi:10.1074/jbc.m010486200
- Kondapalli, C., Kazlauskaitė, A., Zhang, N., Woodroof, H. I., Campbell, D. G., Gourlay, R., et al. (2012). PINK1 Is Activated by Mitochondrial Membrane Potential Depolarization and Stimulates Parkin E3 Ligase Activity by Phosphorylating Serine 65. *Open Biol.* 2 (MAY), 120080. doi:10.1098/rsob.120080
- Korolchuk, V. I., Menzies, F. M., and Rubinsztein, D. C. (2010). Mechanisms of Cross-Talk between the Ubiquitin-Proteasome and Autophagy-Lysosome Systems. *FEBS Lett.* 584 (7), 1393–1398. doi:10.1016/j.febslet.2009.12.047
- Koyano, F., Okatsu, K., Kosako, H., Tamura, Y., Go, E., Kimura, M., et al. (2014). Ubiquitin Is Phosphorylated by PINK1 to Activate Parkin. *Nature* 510 (7503), 162–166. doi:10.1038/nature13392
- Lee, C. A., and Blackstone, C. (2020). ER Morphology and Endo-Lysosomal Crosstalk: Functions and Disease Implications. *Biochim. Biophys. Acta Mol. Cel Biol Lipids* 1865 (1), 158544. doi:10.1016/j.bbalip.2019.158544
- Lee, D. H., and Goldberg, A. L. (1998). Proteasome Inhibitors: Valuable New Tools for Cell Biologists. *Trends Cel Biol.* 8 (10), 397–403. doi:10.1016/s0962-8924(98)01346-4
- Leitman, J., Shenkman, M., Gofman, Y., Shtern, N. O., Ben-Tal, N., Hendershot, L. M., et al. (2014). Herp Coordinates Compartmentalization and Recruitment of HRD1 and Misfolded Proteins for ERAD. *MBoC* 25 (7), 1050–1060. doi:10.1091/mbc.e13-06-0350
- Liao, Y., Duan, B., Zhang, Y., Zhang, X., and Xia, B. (2019). Excessive ER-Phagy Mediated by the Autophagy Receptor FAM134B Results in ER Stress, the Unfolded Protein Response, and Cell Death in HeLa Cells. *J. Biol. Chem.* 294 (52), 20009–20023. doi:10.1074/jbc.ra119.008709
- Marzec, M., Eletto, D., and Argon, Y. (2012). GRP94: An HSP90-like Protein Specialized for Protein Folding and Quality Control in the Endoplasmic Reticulum. *Biochim. Biophys. Acta (Bba) - Mol. Cel Res.* 1823 (3), 774–787. doi:10.1016/j.bbamcr.2011.10.013
- Mejlvang, J., Olsvik, H., Svenning, S., Bruun, J.-A., Abudu, Y. P., Larsen, K. B., et al. (2018). Starvation Induces Rapid Degradation of Selective Autophagy Receptors by Endosomal Microautophagy. *J. Cel Biol.* 217 (10), 3640–3655. doi:10.1083/jcb.201711002
- Miettinen, T. P., and Björklund, M. (2015). Mevalonate Pathway Regulates Cell Size Homeostasis and Proteostasis through Autophagy. *Cel Rep.* 13 (11), 2610–2620. doi:10.1016/j.celrep.2015.11.045
- Miura, H., Hashida, K., Sudo, H., Awa, Y., Takarada-Iemata, M., Kokame, K., et al. (2010). Deletion of Herp Facilitates Degradation of Cytosolic Proteins. *Genes Cells* 15 (8), 843–853. doi:10.1111/j.1365-2443.2010.01422.x
- Mizushima, N., Levine, B., Cuervo, A. M., and Klionsky, D. J. (2008). Autophagy Fights Disease through Cellular Self-Digestion. *Nature* 451 (7182), 1069–1075. doi:10.1038/nature06639
- Mizushima, N., Yoshimori, T., and Ohsumi, Y. (2011). The Role of Atg Proteins in Autophagosome Formation. *Annu. Rev. Cel Dev. Biol.* 27, 107–132. doi:10.1146/annurev-celbio-092910-154005
- Mollazadeh, H., Atkin, S. L., Butler, A. E., Ruscica, M., Sirtori, C. R., and Sahebkar, A. (2018). The Effect of Statin Therapy on Endoplasmic Reticulum Stress. *Pharmacol. Res.* 137, 150–158. doi:10.1016/j.phrs.2018.10.006
- Moreau, K., Luo, S., and Rubinsztein, D. C. (2010). Cytoprotective Roles for Autophagy. *Curr. Opin. Cel Biol.* 22 (2), 206–211. doi:10.1016/j.cob.2009.12.002
- Murrow, L., and Debnath, J. (2013). Autophagy as a Stress-Response and Quality-Control Mechanism: Implications for Cell Injury and Human Disease. *Annu. Rev. Pathol. Mech. Dis.* 8, 105–137. doi:10.1146/annurev-pathol-020712-163918
- Neeffes, J., Jongsma, M. M. L., and Berlin, I. (2017). Stop or Go? Endosome Positioning in the Establishment of Compartment Architecture, Dynamics, and Function. *Trends Cel Biol.* 27 (8), 580–594. doi:10.1016/j.tcb.2017.03.002
- Ou, W.-J., Bergeron, J. J. M., Li, Y., Kang, C. Y., and Thomas, D. Y. (1995). Conformational Changes Induced in the Endoplasmic Reticulum Luminal Domain of Calnexin by Mg-ATP and Ca²⁺. *J. Biol. Chem.* 270 (30), 18051–18059. doi:10.1074/jbc.270.30.18051
- Pathak, R. K., Luskey, K. L., and Anderson, R. G. (1986). Biogenesis of the Crystallin Endoplasmic Reticulum in UT-1 Cells: Evidence that Newly Formed Endoplasmic Reticulum Emerges from the Nuclear Envelope. *J. Cel Biol.* 102 (6), 2158–2168. doi:10.1083/jcb.102.6.2158
- Quiroga, C., Gatica, D., Paredes, F., Bravo, R., Troncoso, R., Pedrozo, Z., et al. (2013). Herp Depletion Protects from Protein Aggregation by Up-Regulating Autophagy. *Biochim. Biophys. Acta (Bba) - Mol. Cel Res.* 1833 (12), 3295–3305. doi:10.1016/j.bbamcr.2013.09.006
- Rothenberg, C., Srinivasan, D., Mah, L., Kaushik, S., Peterhoff, C. M., Ugolino, J., et al. (2010). Ubiquitin Functions in Autophagy and Is Degraded by Chaperone-Mediated Autophagy. *Hum. Mol. Genet.* 19 (16), 3219–3232. doi:10.1093/hmg/ddq231
- Sai, X., Kokame, K., Shiraishi, H., Kawamura, Y., Miyata, T., Yanagisawa, K., et al. (2003). The Ubiquitin-like Domain of Herp Is Involved in Herp Degradation, but Not Necessary for its Enhancement of Amyloid Beta-Protein Generation. *FEBS Lett.* 553 (1–2), 151–156. doi:10.1016/s0014-5793(03)01009-3
- Sauvé, V., Sung, G., Soya, N., Kozlov, G., Blaimschein, N., Miotto, L. S., et al. (2018). Mechanism of Parkin Activation by Phosphorylation. *Nat. Struct. Mol. Biol.* 25 (7), 623–630. doi:10.1038/s41594-018-0088-7
- Schindelin, J., Arganda-Carreras, I., Frise, E., Kaynig, V., Longair, M., Pietzsch, T., et al. (2012). Fiji: An Open-Source Platform for Biological-Image Analysis. *Nat. Methods* 9 (7), 676–682. doi:10.1038/nmeth.2019
- Schuck, S., Prinz, W. A., Thorn, K. S., Voss, C., and Walter, P. (2009). Membrane Expansion Alleviates Endoplasmic Reticulum Stress Independently of the Unfolded Protein Response. *J. Cel Biol.* 187 (4), 525–536. doi:10.1083/jcb.200907074
- Schulz, J., Avci, D., Queisser, M. A., Gutschmidt, A., Dreher, L. S., Fenech, E. J., et al. (2017). Conserved Cytoplasmic Domains Promote Hrd1 Ubiquitin Ligase Complex Formation for ER-Associated Degradation (ERAD). *J. Cel Sci* 130 (19), 3322–3335. doi:10.1242/jcs.206847
- Schulze, A., Standera, S., Buerger, E., Kikkert, M., van Voorden, S., Wiertz, E., et al. (2005). The Ubiquitin-Domain Protein HERP Forms a Complex with Components of the Endoplasmic Reticulum Associated Degradation Pathway. *J. Mol. Biol.* 354 (5), 1021–1027. doi:10.1016/j.jmb.2005.10.020
- Sebt, S., Prebois, C., Perez-Gracia, E., Bauvy, C., Desmots, F., Pirot, N., et al. (2014). BAT3 Modulates P300-dependent Acetylation of P53 and Autophagy-Related Protein 7 (ATG7) during Autophagy. *Proc. Natl. Acad. Sci.* 111 (11), 4115–4120. doi:10.1073/pnas.1313618111
- Sentürk, M., Lin, G., Zuo, Z., Mao, D., Watson, E., and Mikos, A. G., (2019). Ubiquitins Regulates Autophagic Flux through MTOR Signalling and Lysosomal Acidification. *Nat. Cel Biol.* 21 (3), 384–396. doi:10.1038/s41556-019-0281-x
- Shi, X., Han, L., Sun, T., Zhang, F., Ji, S., Zhang, M., et al. (2020). Silencing UHRF1 Enhances Cell Autophagy to Prevent Articular Chondrocytes from Apoptosis in Osteoarthritis through PI3K/AKT/MTOR Signaling Pathway. *Biochem. Biophysical Res. Commun.* 529 (4), 1018–1024. doi:10.1016/j.bbrc.2020.06.032
- Shekel, P. A., Fabian-Fine, R., and Kandel, E. R. (2000). Mouse VAP33 Is Associated with the Endoplasmic Reticulum and Microtubules. *Proc. Natl. Acad. Sci.* 97 (3), 1101–1106. doi:10.1073/pnas.97.3.1101

- Swaney, D. L., Rodríguez Mias, R. A., and Villén, J. (2015). Phosphorylation of Ubiquitin at Ser65 Affects its Polymerization, Targets, and Proteome Wide Turnover. *EMBO Rep.* 16 (9), 1131–1144. doi:10.15252/embr.201540298
- Tanida, I., Ueno, T., and Kominami, E. (2008). LC3 and Autophagy. *Methods Mol. Biol.* 445, 77–88. doi:10.1007/978-1-59745-157-4_4
- Tapia, D., Jiménez, T., Zamora, C., Espinoza, J., Rizzo, R., González-Cárdenas, A., et al. (2019). KDEL Receptor Regulates Secretion by Lysosome Relocation- and Autophagy-dependent Modulation of Lipid-Droplet Turnover. *Nat. Commun.* 10 (1), 735. doi:10.1038/s41467-019-08501-w
- Thastrup, O., Cullen, P. J., Drøbak, B. K., Hanley, M. R., and Dawson, A. P. (1990). Thapsigargin, a Tumor Promoter, Discharges Intracellular Ca²⁺ Stores by Specific Inhibition of the Endoplasmic Reticulum Ca²⁺-ATPase. *Proc. Natl. Acad. Sci. U S A.* 87 (7), 2466–2470. doi:10.1073/pnas.87.7.2466
- Thayer, J. A., Awad, O., Hegdekar, N., Sarkar, C., Tesfay, H., Burt, C., et al. (2020). The PARK10 Gene USP24 Is a Negative Regulator of Autophagy and ULK1 Protein Stability. *Autophagy* 16 (1), 140–153. doi:10.1080/15548627.2019.1598754
- Toledo Pinto, T. G., Batista-Silva, L. R., Medeiros, R. C. A., Lara, F. A., and Moraes, M. O. (2018). Type I Interferons, Autophagy and Host Metabolism in Leprosy. *Front. Immunol.* 9, 806. doi:10.3389/fimmu.2018.00806
- Toulmay, A., and Prinz, W. A. (2011). Lipid Transfer and Signaling at Organelle Contact Sites: The Tip of the Iceberg. *Curr. Opin. Cell Biol.* 23 (4), 458–463. doi:10.1016/j.cceb.2011.04.006
- Tsubuki, S., Saito, Y., Tomioka, M., Ito, H., and Kawashima, S. (1996). Differential Inhibition of Calpain and Proteasome Activities by Peptidyl Aldehydes of Di-leucine and Tri-leucine. *J. Biochem.* 119 (3), 572–576. doi:10.1093/oxfordjournals.jbchem.a021280
- Vabulas, R. M., and Hartl, F. U. (2005). Protein Synthesis upon Acute Nutrient Restriction Relies on Proteasome Function. *Science* 310 (5756), 1960–1963. doi:10.1126/science.1121925
- Valm, A. M., Cohen, S., Legant, W. R., Melunis, J., Hershberg, U., Wait, E., et al. (2017). Applying Systems-Level Spectral Imaging and Analysis to Reveal the Organelle Interactome. *Nature* 546 (7656), 162–167. doi:10.1038/nature22369
- Van Der Laan, S. W., Harshfield, E. L., Hemerich, D., Stacey, D., Wood, A. M., and Asselbergs, F. W. (2018). From Lipid Locus to Drug Target through Human Genomics. *Cardiovasc. Res.* 114 (9), 1258–1270. doi:10.1093/cvr/cvy120
- VerPlank, J. J. S., Lokireddy, S., Zhao, J., and Goldberg, A. L. (2019). 26S Proteasomes Are Rapidly Activated by Diverse Hormones and Physiological States that Raise cAMP and Cause Rpn6 Phosphorylation. *Proc. Natl. Acad. Sci. USA* 116 (10), 4228–4237. doi:10.1073/pnas.1809254116
- Walczak, M., and Martens, S. (2013). Dissecting the Role of the Atg12-Atg5-Atg16 Complex during Autophagosome Formation. *Autophagy* 9 (3), 424–425. doi:10.4161/auto.22931
- Wauer, T., Swatek, K. N., Wagstaff, J. L., Gladkova, C., Pruneda, J. N., Michel, M. A., et al. (2015). Ubiquitin Ser65 Phosphorylation Affects Ubiquitin Structure, Chain Assembly and Hydrolysis. *Embo J.* 34 (3), 307–325. doi:10.15252/emboj.201489847
- Wiest, D. L., Burkhardt, J. K., Hester, S., Hortsch, M., Meyer, D. I., and Argon, Y. (1990). Membrane Biogenesis during B Cell Differentiation: Most Endoplasmic Reticulum Proteins Are Expressed Coordinately. *J. Cell Biol.* 110 (5), 1501–1511. doi:10.1083/jcb.110.5.1501
- Wu, Y., Ma, C., Zhao, H., Zhou, Y., Chen, Z., and Wang, L. (2018). Alleviation of Endoplasmic Reticulum Stress Protects against Cisplatin-Induced Ovarian Damage. *Reprod. Biol. Endocrinol.* 16 (1), 85. doi:10.1186/s12958-018-0404-4
- Xu, F., Du, W., Zou, Q., Wang, Y., Zhang, X., Xing, X., et al. (2021). COPII Mitigates ER Stress by Promoting Formation of ER Whorls. *Cell Res* 31 (2), 141–156. doi:10.38/s41422-020-00416-2
- Xu, H., and Ren, D. (2015). Lysosomal Physiology. *Annu. Rev. Physiol.* 77, 57–80. doi:10.1146/annurev-physiol-021014-071649
- Yan, L., Liu, W., Zhang, H., Liu, C., Shang, Y., Ye, Y., et al. (2014). Ube2g2-Gp78-Mediated HERP Polyubiquitylation Is Involved in ER Stress Recovery. *J. Cell Sci* 127 (7), 1417–1427. doi:10.1242/jcs.135293
- Yang, H., Ni, H.-M., Guo, F., Ding, Y., Shi, Y.-H., Lahiri, P., et al. (2016). Sequestosome 1/P62 Protein Is Associated with Autophagic Removal of Excess Hepatic Endoplasmic Reticulum in Mice. *J. Biol. Chem.* 291 (36), 18663–18674. doi:10.1074/jbc.m116.739821
- Yang, Y., and Klionsky, D. J. (2020). A Novel Role of UBQLNs (Ubiquilins) in Regulating Autophagy, MTOR Signaling and V-ATPase Function. *Autophagy* 16 (1), 1–2. doi:10.1080/15548627.2019.1665293
- Yin, Y., Seifert, A., Chua, J. S., Maure, J.-F., Golebiowski, F., and Hay, R. T. (2012). SUMO-targeted Ubiquitin E3 Ligase RNF4 Is Required for the Response of Human Cells to DNA Damage. *Genes Dev.* 26 (11), 1196–1208. doi:10.1101/gad.189274.112
- Yoshida, H., Matsui, T., Yamamoto, A., Okada, T., and Mori, K. (2001). XBP1 mRNA Is Induced by ATF6 and Spliced by IRE1 in Response to ER Stress to Produce a Highly Active Transcription Factor. *Cell* 107 (7), 881–891. doi:10.1016/s0092-8674(01)00611-0
- Yoshii, S. R., Kuma, A., Akashi, T., Hara, T., Yamamoto, A., Kurikawa, Y., et al. (2016). Systemic Analysis of Atg5-Null Mice Rescued from Neonatal Lethality by Transgenic ATG5 Expression in Neurons. *Dev. Cell* 39 (1), 116–130. doi:10.1016/j.devcel.2016.09.001
- Yu, H., and Matouschek, A. (2017). Recognition of Client Proteins by the Proteasome. *Annu. Rev. Biophys.* 46, 149–173. doi:10.1146/annurev-biophys-070816-033719
- Zhang, T., Lu, D., Yang, W., Shi, C., Zang, J., Shen, L., et al. (2018). HMG-CoA Reductase Inhibitors Relieve Endoplasmic Reticulum Stress by Autophagy Inhibition in Rats with Permanent Brain Ischemia. *Front. Neurosci.* 12 (JUN), 405. doi:10.3389/fnins.2018.00405
- Zhang, Youzhi. (2020). Simvastatin Improves Lysosome Function via Enhancing Lysosome Biogenesis in Endothelial Cells. *Front. Biosci. - Landmark* 25 (2), 283–298. doi:10.2741/4807
- Zhu, K., Dunner, K., and McConkey, D. J. (2010). Proteasome Inhibitors Activate Autophagy as a Cytoprotective Response in Human Prostate Cancer Cells. *Oncogene* 29 (3), 451–462. doi:10.1038/onc.2009.343

Conflict of Interest: The authors declare that the research was conducted in the absence of any commercial or financial relationships that could be construed as a potential conflict of interest.

Publisher's Note: All claims expressed in this article are solely those of the authors and do not necessarily represent those of their affiliated organizations or those of the publisher, the editors, and the reviewers. Any product that may be evaluated in this article, or claim that may be made by its manufacturer, is not guaranteed or endorsed by the publisher.

Copyright © 2022 Vargas, Cortés, Arias-Muñoz, Hernández, Cerda-Troncoso, Hernández, González, Tatham, Bustamante, Retamal, Cancino, Varas-Godoy, Hay, Rojas-Fernández, Cavieres and Burgos. This is an open-access article distributed under the terms of the Creative Commons Attribution License (CC BY). The use, distribution or reproduction in other forums is permitted, provided the original author(s) and the copyright owner(s) are credited and that the original publication in this journal is cited, in accordance with accepted academic practice. No use, distribution or reproduction is permitted which does not comply with these terms.